

CANCER

FBXO42 facilitates Notch signaling activation and global chromatin relaxation by promoting K63-linked polyubiquitination of RBPJ

Hua Jiang^{1,2,3†}, Weixiang Bian^{1,2,3†}, Yue Sui^{1,2,3†}, Huanle Li^{2,3}, Han Zhao^{2,3}, Wenqi Wang⁴, Xu Li^{1,2,3*}

Dysregulation of the Notch–RBPJ (recombination signal-binding protein of immunoglobulin kappa J region) signaling pathway has been found associated with various human diseases including cancers; however, precisely how this key signaling pathway is fine-tuned via its interactors and modifications is still largely unknown. In this study, using a proteomic approach, we identified F-box only protein 42 (FBXO42) as a previously unidentified RBPJ interactor. FBXO42 promotes RBPJ polyubiquitination on lysine-175 via lysine-63 linkage, which enhances the association of RBPJ with chromatin remodeling complexes and induces a global chromatin relaxation. Genetically depleting *FBXO42* or pharmacologically targeting its E3 ligase activity attenuates the Notch signaling–related leukemia development in vivo. Together, our findings not only revealed FBXO42 as a critical regulator of the Notch pathway by modulating RBPJ-dependent global chromatin landscape changes but also provided insights into the therapeutic intervention of the Notch pathway for leukemia treatment.

INTRODUCTION

The Notch signaling pathway is one of the most commonly dysregulated pathways in cancer. Alterations include activating mutations and amplification of Notch pathway activity, leading to the progression of cancers, especially T cell acute lymphoblastic leukemia/lymphoma (T-ALL) (1), chronic lymphocytic leukemia (CLL) (2), diffuse large B cell lymphoma (DLBCL) (3), head and neck squamous cell carcinoma (HNSCC) (4, 5), and breast cancers (6, 7). Therapeutic strategies to modulate Notch pathway function include chemical and immunological targeting of NOTCH receptors, Delta ligands, and γ -secretases (8–10). Although the Notch pathway has been studied in past decades, the use of pharmacological compounds targeting Notch activity in clinical settings is still insufficient, especially in *NOTCH*-activated T cell leukemia. To date, γ -secretase inhibitors have been the most extensively explored potential anti-cancer agents in these contexts. However, because of the side effects induced by γ -secretase inhibitors in clinical settings (11) and because mutant *NOTCH* does not require γ -secretase cleavage to be activated (1), the need to develop new strategies by identifying novel molecular targets, especially components downstream of Notch activation, remains urgent.

Recombination signal-binding protein of immunoglobulin kappa J region (RBPJ), a transcription factor in the Notch signaling pathway, plays a dual role in regulating Notch signaling. In the absence of the Notch intracellular domain (NICD), RBPJ acts as a transcriptional repressor of Notch target genes, exerting its effect by interacting with corepressor complexes such as histone deacetylases (HDACs) (12), lysine-specific histone demethylase 1A

(KDM1A or LSD1) (13), and lethal (3) malignant brain tumor–like protein 3 (L3MBTL3) (14). Upon Notch activation, RBPJ associates with the NICD and Mastermind-like protein (MAMLs) to form a ternary complex, recruiting coactivators such as the histone acetyltransferases p300 and GCN5 and triggering the transcription of Notch target genes (15).

Despite the progress made in delineating the molecular structures of the transcriptional complex in the past decade, the mechanism of RBPJ function switching remains unclear, making it difficult to target the Notch transcription step. The depletion of RBPJ leads to Notch signaling inactivation in certain cellular contexts (16) and to Notch signaling activation in other contexts (17), making pharmacologically targeting RBPJ in Notch-related cancers very risky.

RBPJ/NICD dimerization is suspected to be a stabilizing event enabling RBPJ binding (18–20); however, the DNA binding affinity of RBPJ is unexpectedly low [dissociation constant (K_d) of $\sim 1 \mu\text{M}$] (21), and the binding of NICD to RBPJ does not influence RBPJ-binding affinity for DNA (21). It remains to be elucidated whether the plasticity of DNA binding by RBPJ is due to cofactors that can sense chromatin structure (22, 23) or whether RBPJ cooperates with other DNA binding proteins to prolong its association with chromatin (24, 25). In any case, the role of RBPJ is controversial and context dependent, and the mechanism by which the RBPJ transcriptional switch is fine-tuned remains to be elucidated.

In this study, we established a detailed RBPJ interactome via tandem affinity purification coupled with mass spectrometry (TAP-MS) and explored the potential regulators critical for RBPJ transcriptional activities. We found that F-box only protein 42 (FBXO42) physically and functionally interacted with RBPJ, mediating its K63-linked polyubiquitination and contributing to its binding to chromatin, the conformation of which was subsequently opened, and Notch signaling activation. Both genetic knockout (KO) of *FBXO42* and pharmacological inhibition of FBXO42 action alleviated leukemia progression in vivo, exhibiting therapeutic value in Notch-associated disease.

Copyright © 2022 The Authors, some rights reserved; exclusive licensee American Association for the Advancement of Science. No claim to original U.S. Government Works. Distributed under a Creative Commons Attribution NonCommercial License 4.0 (CC BY-NC).

¹Fudan University, Shanghai 310018, China. ²Key Laboratory of Structural Biology of Zhejiang Province, School of Life Sciences, Westlake University, Hangzhou 310024, Zhejiang, China. ³Westlake Laboratory of Life Sciences and Biomedicine, Hangzhou 310024, Zhejiang, China. ⁴Department of Developmental and Cell Biology, University of California, Irvine, Irvine, CA 92697, USA.

*Corresponding author. Email: lixu@westlake.edu.cn

†These authors contributed equally to this work.

RESULTS**Proteomic analysis of the RBPJ interaction network identifies FBXO42 as a critical regulator of Notch signaling**

To gain a comprehensive understanding of the transcriptional regulation of the Notch pathway and identify novel RBPJ interactors, we established a RBPJ protein interaction network using TAP-MS in human embryonic kidney (HEK) 293T cells. HEK293T cells have broad spectrum of protein expression (26), and they are easy to grow and accessible for transfection. The MS analysis of purified protein extracts revealed the successful purification of RBPJ with a 570 and 381 peptide-spectrum match against RBPJ, respectively. We analyzed the MS results using the MUSE algorithm (27) and established a high-confidence map of RBPJ interactors (Fig. 1A). Functional annotation and pathway enrichment assays showed that RBPJ interactors are highly involved in embryonic development, cell fate decisions, and transcriptional regulation (fig. S1, A to C), which is consistent with their roles played in Notch signaling. We picked several of the strongest RBPJ-interacting proteins identified in this study for a coimmunoprecipitation assay to validate their interactions with RBPJ (fig. S1D). All the interactors tested interacted with RBPJ, indicating that this interaction network was reliable (fig. S1D). CRISPR-Cas9-mediated KO screening of the strongest RBPJ interactors revealed the top positive and negative regulators of Notch signaling. Knocking out *L3MBTL3*, a previously reported negative regulator of RBPJ (14), increased Notch target gene expression (Fig. 1, B and C), and knocking out *FBXO42* significantly decreased Notch target gene expression (Fig. 1, D and E). Moreover, knocking out *FBXO42* impaired RBPJ binding to *HES1/5* promoter regions and constructed 8× RBPJ-binding site (Fig. 1, F and G), indicating that *FBXO42* may regulate RBPJ transcriptional activities by direct binding.

Dysregulation of Notch signaling has been linked with various cancer types, including T-ALL, DLBCL, HNSCC, and breast cancers (1, 3–7). We found that *FBXO42* was highly expressed in Notch-activated T cell leukemia, DLBCL, and breast cancer, and its expression was down-regulated in Notch-inactivated HNSCC (Fig. 1, H to J, and fig. S1, E and F). It was also highly expressed in various leukemia and breast cancer cell lines (Fig. 1K), especially in ALL cell lines (Fig. 1L). To further establish the correlation between *FBXO42* expression and Notch signaling in patients, we analyzed publicly available cancer omics data using The Cancer Genome Atlas (TCGA) dataset and UALCAN database (28) and found that *FBXO42* expression is highly correlated with the expression of Notch target genes *HES1*, *MYC*, *HES5*, *HEY1*, *HEY2*, and *HEYL* in patients with DLBCL, acute myeloid leukemia, and ALL (Fig. 1, M and N, and fig. S1G). Together, these data suggested a potential role of *FBXO42* as an important positive regulator of Notch signaling.

FBXO42 directly interacts with RBPJ

FBXO42 is a substrate recognition component of the S-phase kinase-associated protein 1 (SKP1)–Cullin-1 (CUL1)–F-box protein (SCF)–type E3 ligase complex, which has been previously reported to promote p53 ubiquitination and degradation (29). To determine whether RBPJ and *FBXO42* directly interact, we performed reciprocal TAP-MS using *FBXO42* as the bait and established an *FBXO42* interaction network (Fig. 2A). A Kyoto Encyclopedia of Genes and Genomes (KEGG) enrichment analysis indicated the potential involvement of *FBXO42* under many pathological conditions (Fig. 2B). We identified several previously reported *FBXO42* interactors, including SKP1, CUL1, and COP9 signalosome complex subunit (COPS) family members,

which are involved in the deneddylation of the cullin subunits in SCF-type E3 ligase complexes (30, 31). RBPJ has also been repeatedly identified as a strong interactor of *FBXO42* (Fig. 2A), indicating that *FBXO42* forms a stable protein complex with RBPJ. Although there is little overlap between RBPJ- and *FBXO42*-interacting proteins, the functions of these proteins overlap to a high degree (Fig. 2C), indicating that *FBXO42* may specifically facilitate RBPJ transcriptional activity.

We further validated the interaction between *FBXO42* and RBPJ using antibodies against endogenous *FBXO42* or RBPJ (Fig. 2, D and E) and epitope-tagged RBPJ and *FBXO42* (Fig. 2, F and G). *FBXO42* and RBPJ strongly interacted with each other (Fig. 2, D to G). To estimate the dynamic binding parameters that underlie the RBPJ/*FBXO42* interaction in vitro, we performed a biomolecular interaction analysis with purified recombinant RBPJ and *FBXO42* proteins (Fig. 2H). *FBXO42* interacted with RBPJ with very high affinity ($K_d = 47$ nM) in vitro (Fig. 2I). To identify the binding regions on RBPJ and *FBXO42*, we generated a series of domain deletion mutants of RBPJ and *FBXO42* (Fig. 2, J and K). We found that the N-terminal domain (NTD; amino acids 1 to 178) of RBPJ (Fig. 2L) and the Kelch domain (amino acids 101 to 350) of *FBXO42* (Fig. 2M) are critical for their interaction. Consistently, a strong interaction between RBPJ-NTD and *FBXO42*-Kelch domain was observed (Fig. 2N). Together, these data demonstrated the direct interaction between RBPJ and *FBXO42* both in vitro and in cells, which was mediated by the NTD of RBPJ and the Kelch domain of *FBXO42*.

FBXO42 promotes RBPJ K63-linked polyubiquitination and positively regulates Notch signaling

As *FBXO42* belongs to the SCF complex, we wondered whether *FBXO42* is involved in the ubiquitination of RBPJ. We found that *FBXO42* promoted RBPJ polyubiquitination, which was markedly attenuated upon *FBXO42* depletion (Fig. 3, A and B, and fig. S2A). The *FBXO42* F-box domain, which links *FBXO42* to other components in the SCF complex, was required for RBPJ polyubiquitination (Fig. 3C). The Kelch domain of *FBXO42*, which mediates its interaction with RBPJ, was also required for RBPJ polyubiquitination (fig. S2B). Overexpressing NICD slightly increased RBPJ polyubiquitination, suggesting a potential role of Notch signaling activation in promoting RBPJ polyubiquitination (Fig. 3D). Using ubiquitin mutants in which only a single wild-type (WT) K residue was retained, while all the other K residues were replaced with arginine (R) residues, we found only overexpressing K63 ubiquitin with *FBXO42* promoted substantial RBPJ polyubiquitylation, indicating that *FBXO42* specifically promotes RBPJ K63-linked polyubiquitination (Fig. 3E).

To map the ubiquitination site(s) in RBPJ, we performed MS and analyzed the RBPJ ubiquitination profile in the presence and absence of *FBXO42*. Overexpression of *FBXO42* greatly promoted RBPJ K175 ubiquitination, as indicated by MS (Fig. 3F). This modification was detectable in WT cells but not in *FBXO42* KO cells (fig. S2C). We also constructed mutants carrying K-to-R mutations in potential ubiquitination sites in RBPJ as indicated by the Phosphosite public database (www.phosphosite.org) and detected their ubiquitination intensity. Only the K175R mutant significantly abrogated *FBXO42*-mediated RBPJ polyubiquitination (Fig. 3G and fig. S2D). The K175 residue is evolutionally conserved, suggesting that homologous sites in other organisms may be similarly modified (Fig. 3H). K175 ubiquitination did not affect the turnover rate of RBPJ, indicating that it does not mediate RBPJ proteolytic degradation (Fig. 3, I and J). Because *FBXO42* is the substrate-recognizing

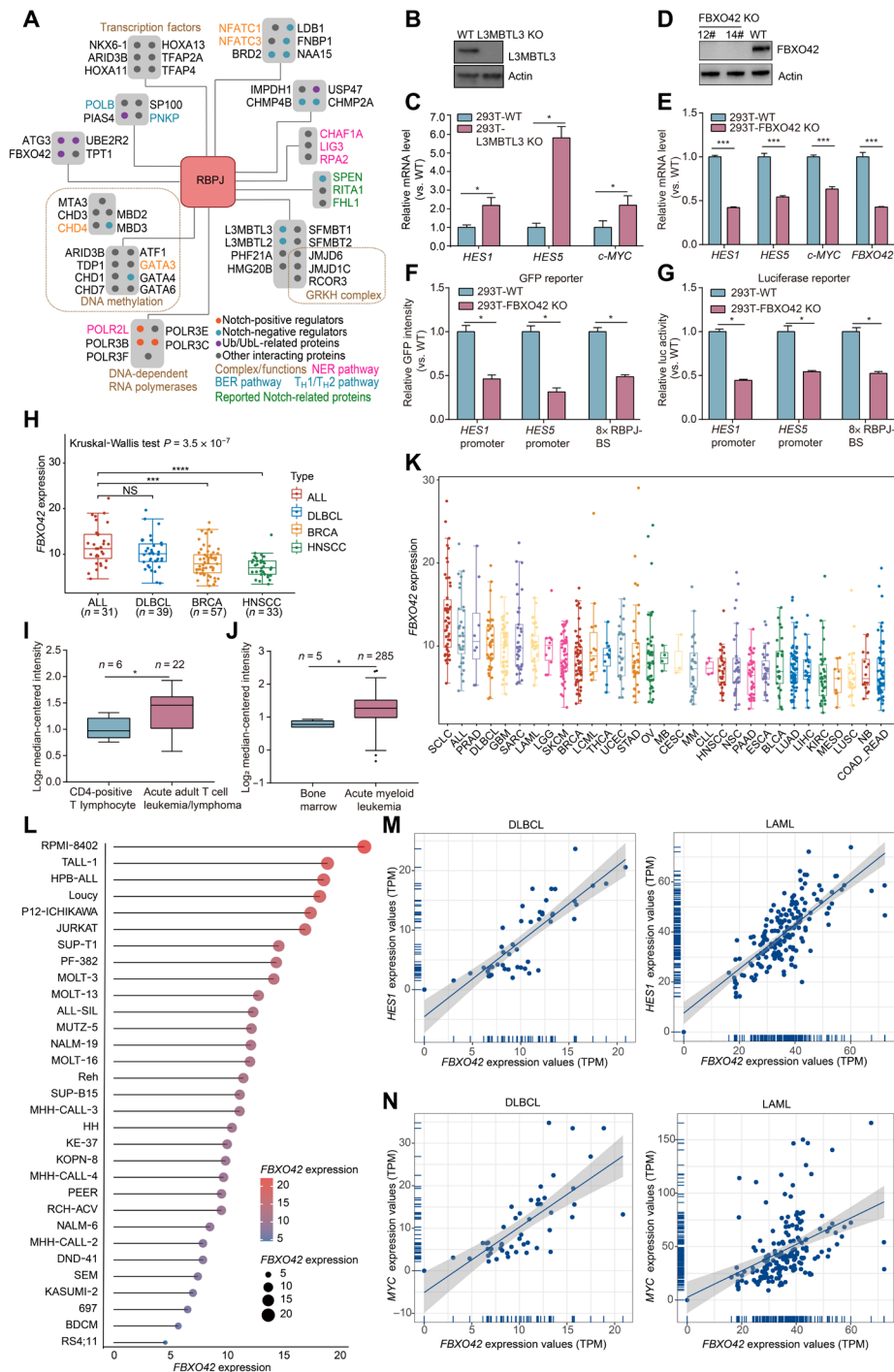


Fig. 1. FBXO42 is a critical interactor of RBPJ and a positive regulator of the Notch pathway. (A) Interaction network of RBPJ. high-confidence interacting proteins (HCIPs) were grouped on the basis of their cellular functions as indicated by Gene Ontology (GO) analysis and a literature search. Ubiquitination (Ub)/ubiquitin-like (Ubl)-related proteins, proteins that are potential positive and negative regulators, are indicated by different colored dots. Signaling pathways and proteins reported to be involved in Notch pathway regulation are indicated by different colored texts. NER, nuclear excision repair; BER, base excision repair; T_H1/T_H2, T helper 1/2 cells. (B and C) Expression of L3MBTL3 (B) and Notch target genes (C) was evaluated in wild-type (WT) and L3MBTL3 KO HEK293T cells. (D and E) Expression of FBXO42 (D) and Notch target genes (E) was evaluated in WT and FBXO42 KO HEK293T cells. (F and G) Green fluorescent protein (GFP) reporter (F) and Luciferase assays (G) were performed to evaluate Notch signaling activities in WT and FBXO42 KO HEK293T cells. RBPJ-BS, RBPJ binding site. (H to J) Expression level of FBXO42 in Notch-related cancers as indicated was analyzed using The Cancer Genome Atlas (TCGA) datasets. (K and L) Expression level of FBXO42 in various cancer cell lines (K) and T-ALL cell lines (L) derived from the Cancer Cell Line Encyclopedia (<https://sites.broadinstitute.org/ccle>). (M and N) Expression correlation of FBXO42 and Notch pathway target genes in patients with DLBCL and acute myeloid leukemia (AML) was analyzed using TCGA dataset and UALCAN database. (B) to (G), n = 3. Quantitative data are presented as means ± SEM from three independent experiments. P values were calculated using two-tailed Student's t tests. *P < 0.05, ***P < 0.001, and ****P < 0.0001. NS, not significant; TPM, transcript per million.

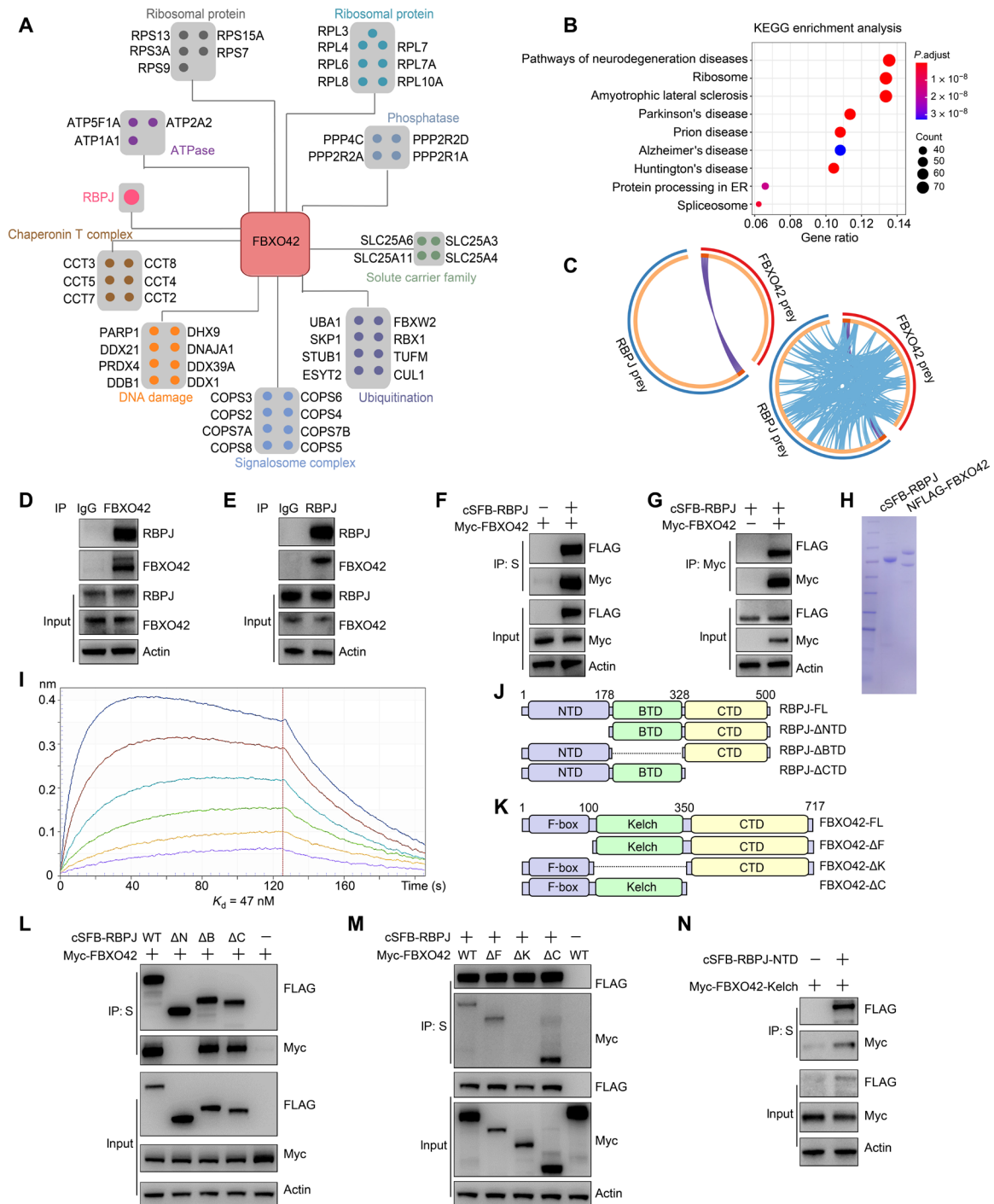


Fig. 2. FBXO42 directly interacts with RBPJ. (A) Interaction network of FBXO42. Top 50 interactors identified in TAP-MS were shown. (B) KEGG enrichment analysis of preys acquired in FBXO42 TAP-MS. ER, endoplasmic reticulum. (C) Circos plot showing overlapping RBPJ and FBXO42 preys. Purple lines link the genes that shared by RBPJ and FBXO42. Blue lines link different genes enriched in the same ontology term. (D and E) HEK293T cell lysates were incubated with immunoglobulin G (IgG) control and antibodies against FBXO42 (D) or RBPJ (E). Five percent lysate was used as the input control. Blots with antibodies recognizing RBPJ, FBXO42, and actin are shown. IP, immunoprecipitation. (F and G) HEK293T cells were cotransfected with Myc-tagged FBXO42 and C-terminal SFB (cSFB)-tagged RBPJ, as indicated. The cell lysates were incubated with S-beads (F) or an anti-Myc antibody (G). (H) Coomassie blue staining of cSFB-RBPJ and FLAG-FBXO42 proteins purified from 293F cells. (I) Biomolecular interaction kinetics curve showing the binding affinity between purified RBPJ and FBXO42 proteins. A final concentration of 225 nM RBPJ was used for binding to the SA (Streptavidin) probe. The colored lines indicate the concentration gradient of FBXO42 (19.5 to 625 nM). (J and K) Schematics showing RBPJ (J) and FBXO42 (K) domain deletion mutants. CTD, C-terminal domain; BTD, β -trefoil domain. (L and M) HEK293T cells were cotransfected with Myc-tagged FBXO42 and cSFB-tagged WT or mutant RBPJ (L) or cSFB-tagged RBPJ and Myc-tagged WT or mutant FBXO42 (M). (N) HEK293T cells were cotransfected with Myc-FBXO42-Kelch domain and cSFB-RBPJ-NTD (N-terminal domain) as indicated. (L to N) Cell lysates were incubated with S-beads. Five percent lysate was used as the input control. (D) to (I) and (L) to (N), $n = 3$.

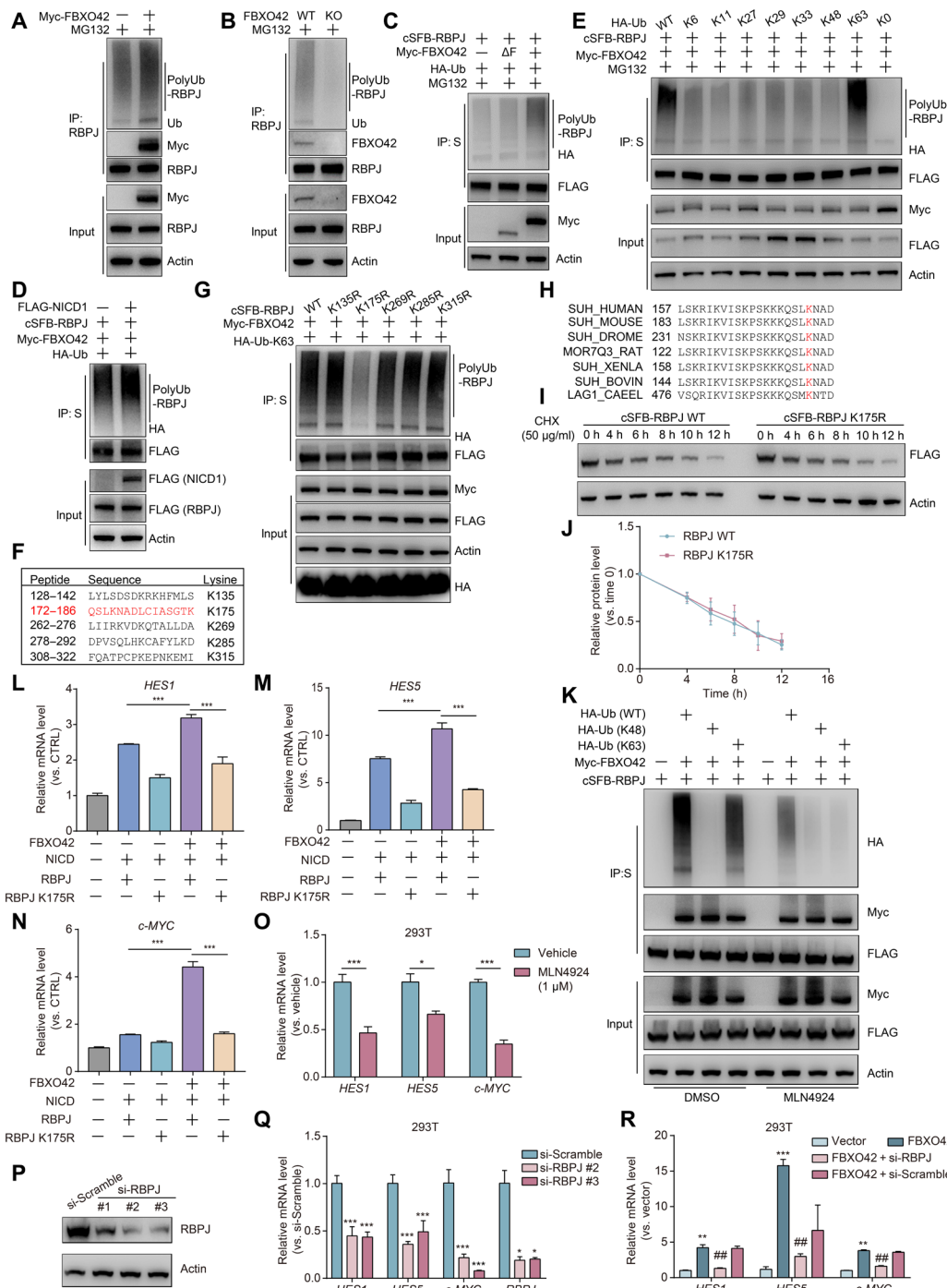


Fig. 3. FBXO42 promotes RBPJ K63-linked polyubiquitination and positively regulates Notch signaling. (A and B) Endogenous RBPJ ubiquitination was measured under FBXO42 overexpression (A) or FBXO42 depletion (B) after IP with antibody against RBPJ and immunoblotted for ubiquitination. (C) cSFB-RBPJ, hemagglutinin (HA)-ubiquitin, and Myc-FBXO42 WT or ΔF mutant were cotransfected into HEK293T cells and analyzed for RBPJ polyubiquitination. (D) RBPJ ubiquitination change under NICD1 overexpression. (E) Determination of RBPJ ubiquitination chain linkage. (F) Sequences of the predicted and identified peptides (the respective lysine residues are indicated) in MS are shown. (G) Evaluating ubiquitination intensity of five cSFB-RBPJ lysine mutants. (H) Sequence alignment of RBPJ in different species showed the conservation of the K175 site. (I) HEK293T cells transfected with cSFB-RBPJ WT or K175R mutant were treated with cycloheximide (CHX) for the indicated times, and the lysates were analyzed by Western blotting. (J) Quantitation of the results shown in (I). (K) Effect of MLN4924 on FBXO42-mediated RBPJ ubiquitination. (L to N) Quantitative polymerase chain reaction (qPCR) analysis of the Notch target genes in HEK293T cells overexpressing FBXO42, RBPJ WT, or K175R mutant. (O) mRNA expression of Notch target genes in cells treated with MLN4924. (P) Efficiency of RBPJ short interfering RNAs (siRNAs). (Q) qPCR analysis of Notch target genes in RBPJ knockdown cells. (R) HEK293T cells were transfected with si-Scramble or si-RBPJ and overexpressed with Myc-FBXO42 and then subjected to qPCR analysis of Notch target gene expression. (A) to (G) and (I) to (R), $n = 3$. Quantitative data are presented as means \pm SEM. P values were calculated using two-tailed Student's t tests or analysis of variance (ANOVA) for multiple comparison. * $P < 0.05$, ** $P < 0.01$, *** $P < 0.001$, and ## $P < 0.01$ versus FBXO42.

component in the SCF complex, we used MLN4924, a small-molecule inhibitor of the Neural precursor cell expressed developmentally down-regulated protein 8 (NEDD8)-activating enzyme, to determine whether the function of FBXO42 can be pharmacologically targeted. MLN4924 inhibits CUL1 neddylation and thus SCF activity and is currently in phase 1 to 3 clinical trials (32, 33). MLN4924 effectively abrogated the FBXO42-mediated K63-linked polyubiquitination of RBPJ (Fig. 3K). To find out whether FBXO42 ubiquitinates other Notch pathway core components to regulate Notch signaling, we analyzed the global ubiquitination changes upon FBXO42 KO and MLN4924 treatment (fig. S2, E to G). None of the core components of Notch pathway other than RBPJ was identified in either FBXO42 interactome (Fig. 2A) or the global ubiquitination analysis (fig. S2, E to G), indicating that FBXO42 regulates Notch pathway mainly through RBPJ.

Ubiquitin conjugation via the K48 linkage is a mark that targets modified proteins for proteasomal degradation, whereas K63-linked conjugation often plays a role in signal transduction (34). Considering that RBPJ is the main transcription factor in Notch signaling, FBXO42 may regulate Notch pathway activation by promoting RBPJ K63-linked ubiquitination. Overexpressing FBXO42 with WT RBPJ, but not the RBPJ K175R mutant, significantly increased the expression of the Notch target genes *HES1*, *HES5*, and *c-MYC* (Fig. 3, L to N), indicating that RBPJ K175 polyubiquitination is required for its transcriptional activity. MLN4924 treatment also suppressed the expression of the aforementioned Notch target genes (Fig. 3O), supporting the idea that FBXO42-mediated K63-linked polyubiquitination of RBPJ is involved in Notch signaling activation. Knocking down RBPJ expression decreased the expression of the Notch target genes *HES1*, *HES5*, and *c-MYC* (Fig. 3, P and Q) and abolished the FBXO42-promoted activation of these genes (Fig. 3R), indicating that FBXO42-promoted Notch activation is RBPJ dependent. Together, these findings suggested that FBXO42 positively regulated Notch signaling by promoting K63-linked polyubiquitination of RBPJ at K175.

FBXO42 regulates RBPJ chromatin association and transcriptional activity

RBPJ is considered to play a dual role in the regulation of Notch signaling. Depletion of RBPJ can result in either the inhibition or activation of Notch target genes, depending on the cellular context (35). To further illustrate the mechanism of RBPJ transcriptional activity regulation, we performed a subcellular fractionation assay and evaluated the level of RBPJ and its ubiquitination in different cellular compartments. Knocking out FBXO42 decreased the levels of nuclear- and chromatin-bound RBPJ while increasing the cytoplasmic RBPJ level (Fig. 4A). The RBPJ K175R mutant also showed less chromatin binding than WT RBPJ (Fig. 4B). Consistently, the ubiquitinated RBPJ was more chromatin associated, which was attenuated by FBXO42 depletion and enhanced with FBXO42 overexpression (fig. S4, A to C), suggesting that FBXO42-mediated polyubiquitination of RBPJ regulated RBPJ association with chromatin.

To further explore the molecular mechanism by which RBPJ transcription is activated, we evaluated the role of FBXO42 in RBPJ cofactor selectivity because the transcriptional activity of RBPJ depends on its interaction with coactivators or corepressors (36). Knocking out FBXO42 suppressed the interaction of RBPJ with the coactivators p300, MAML1, and NICD1 while enhancing its interaction with the corepressor L3MBTL3 (Fig. 4, C and D). The RBPJ K175R mutant showed a cofactor selectivity similar to that after FBXO42 KO (Fig. 4E), indicating that FBXO42-mediated polyubiquitination of

RBPJ regulates RBPJ cofactor preference. Next, we wondered whether FBXO42 directly modulates RBPJ transcriptional activity. Knocking out FBXO42 expression suppressed the histone 3 (H3) K4 methylation and H3K27 acetylation levels of RBPJ, which were rescued by overexpressing WT FBXO42 but not by overexpressing the FBXO42 mutant with its F-box deleted (Fig. 4F).

To further understand whether and how FBXO42-mediated RBPJ K175 ubiquitination affects its transcription activity, we first performed the Cleavage Under Targets and Tagmentation (CUT&Tag) assay in WT and FBXO42 KO cells and identified many classical RBPJ-binding motifs (Fig. 4G) and several consensus motifs of other transcription factors, including E2F1, zinc finger protein 423 (ZNF423), high mobility group nucleosome-binding domain-containing protein 1 (HMGN1), yin and yang 1 (YY1), and zic family member 2 (ZIC2) (fig. S3, D to G), which have been reported to be involved in transcriptional regulation in leukemia (37–41). Knocking out FBXO42 led to a decrease in global RBPJ binding and the chromatin recruitment of RBPJ to its target genes *HES1*, *HES4*, and *MYC* (Fig. 4, H and I). Genes with differential RBPJ-binding affinity after FBXO42 KO were mainly enriched in protein homeostasis, cell behavior, signaling transduction, and Notch-related cancers, consistent with the biological role played by RBPJ (Fig. 4J). Then, we performed CUT&Tag assays using WT RBPJ and its K175R mutant (Fig. 4K and fig. S3, H to J). RBPJ K175R mutant showed a significant decrease in global RBPJ binding to its specific binding sites (Fig. 4K) and the chromatin recruitment of RBPJ to its target genes *HES1*, *HES4*, and *MYC* (fig. S3, H to J). Together, it indicates that, compared with WT RBPJ, the transcriptional activity of its K175R mutant was significantly impaired. We also performed the rescue experiment in RBPJ KO cells using WT RBPJ and its K175R mutant (fig. S3K). WT RBPJ binds to *HES1/5* promoter regions and constructs 8× RBPJ-binding site better than the K175R mutant, as indicated by luciferase reporter assays (fig. S3K), suggesting that RBPJ K175 ubiquitination is essential for RBPJ chromatin association. Together, these data indicated that FBXO42-mediated polyubiquitination of RBPJ regulates RBPJ chromatin association and subsequently regulates its transcriptional activity.

FBXO42 mediates global chromatin remodeling in an RBPJ-dependent manner

Chromatin remodeling is critical for transcriptional regulation (42, 43); therefore, we wondered whether FBXO42 regulates the interactions between RBPJ and chromatin remodeling complexes. Knocking out FBXO42 broadly led to increased interactions between RBPJ and the heterochromatin components HDAC1, LSD1, transcription intermediary factor 1-beta (TRIM28), Chromobox protein homolog 1 (CBX1), and CBX5, which are related to gene silencing (Fig. 5A) (44), and decreased interactions between RBPJ and core components of the SWItch/Sucrose NonFermentable (SWI/SNF) complex, the chromatin remodeling complex involved in transcriptional activation (Fig. 5B). Then, we performed TAP-MS of RBPJ in WT and FBXO42 KO HEK293T cells (Fig. 5C). Consistently, knocking out FBXO42 promoted RBPJ association with heterochromatin components LSD1, TRIM28, CBX1, CBX3, and CBX5, which are related to gene silencing, and decreased the RBPJ association with core components of the SWI/SNF complex, the chromatin remodeling complex involved in transcriptional activation (Fig. 5C). Then, we performed similar assays using WT RBPJ and its K175R mutant. RBPJ K175R mutant pulled down more heterochromatin components such as LSD1, CBX1, CBX3, CBX5 and less core components

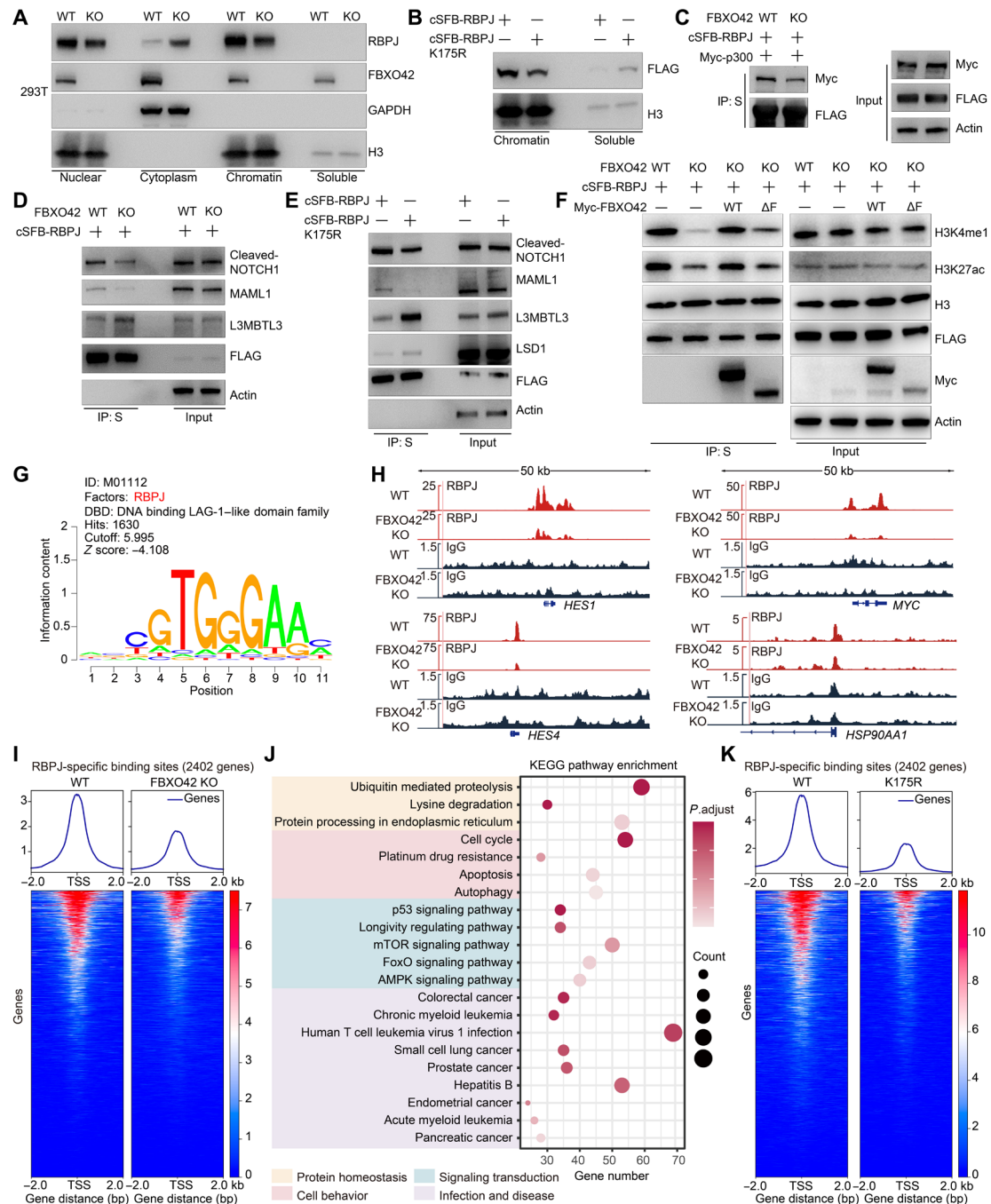


Fig. 4. FBXO42 regulates RBPJ chromatin association and transcriptional activity. (A) WT and FBXO42 KO HEK293T cells were harvested and subjected to subcellular fractionation. The nuclear, cytoplasm, chromatin, and soluble fractions were isolated, and immunoblot analysis was performed. (B) HEK293T cells overexpressing RBPJ WT or K175R were harvested, the chromatin and soluble fractions were isolated, and the immunoblot analyses were performed. (C) WT and FBXO42 KO HEK293T cells were cotransfected with cSFB-RBPJ and Myc-p300. Cell lysates were collected, incubated with S-protein beads, and blotted with antibodies against FLAG- or MYC-epitope tags. (D) WT and FBXO42 KO HEK293T cells were transfected with cSFB-RBPJ and used for S-protein bead pull-down assay, followed by immunoblotting with endogenous antibodies as indicated. (E) HEK293T cells expressing RBPJ WT or its K175R mutant were harvested and used for S-protein bead pull-down assay, followed by immunoblotting with endogenous antibodies as indicated. (F) WT and FBXO42 KO HEK293T cells were transfected with cSFB-RBPJ and Myc-FBXO42 WT or ΔF mutant. Then, the histone modifications were evaluated with Western blotting using antibodies against H3K4me1 and H3K27ac. H3 and actin served as the loading controls. (A) to (F), $n = 3$. (G) WT and FBXO42 KO HEK293T cells were collected for a CUT&Tag assay. Classical RBPJ motif identified in CUT&Tag assay was shown. (H) Representative images of RBPJ-binding sites in known Notch pathway target genes *HES1*, *HES4*, and *MYC* were shown. *HSP90AA1* was used as the negative control. (I) Heatmap showing RBPJ CUT&Tag read densities of WT and FBXO42 KO HEK293T cells. TSS, transcription start site. (J) Signaling pathway enrichment of genes with differential RBPJ-binding affinities based on GO annotation. The size of the dots represents the number of genes associated with the GO term, and the color of the dots represents the adjusted P values. AMPK, adenosine monophosphate-activated protein kinase; mTOR, mammalian target of rapamycin. (K) Heatmap showing CUT&Tag read densities of RBPJ WT and K175R mutant.

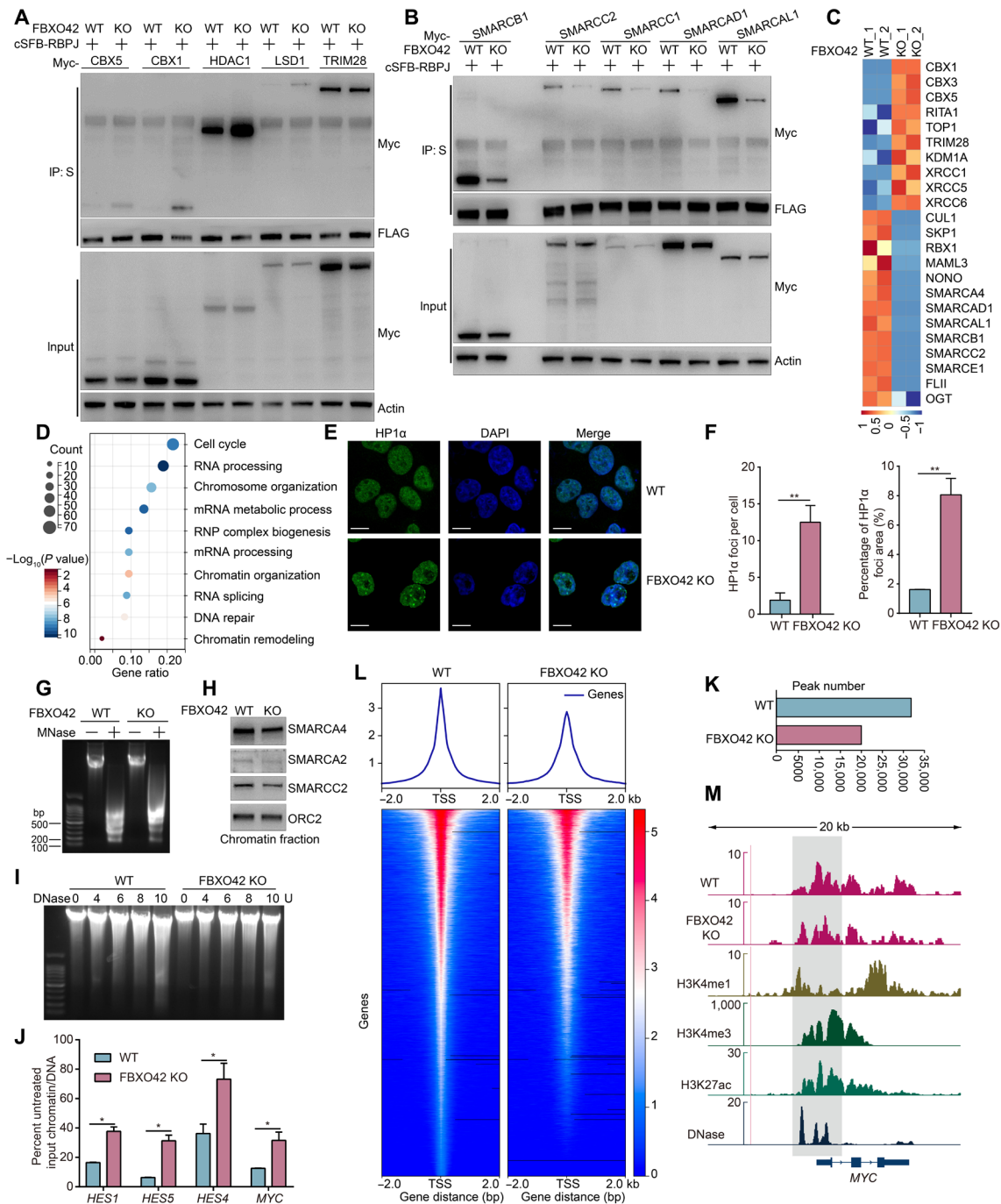


Fig. 5. FBXO42 mediates global chromatin remodeling in an RBPJ-dependent manner. (A) WT and FBXO42 KO cells were cotransfected with cSF-BRPJ– and Myc-tagged constructs encoding epigenetically modified proteins. Then, cell lysates were incubated with S-protein beads and blotted with antibodies against FLAG- or MYC-epitope tags. (B) WT and FBXO42 KO cells were cotransfected with cSF-BRPJ– and Myc-tagged constructs encoding SWI/SNF complex proteins. Then, the cells were harvested and analyzed as described in (A). (C) Heatmap showing the differential interaction between chromatin factors and RBPJ in WT and FBXO42 KO cells as identified by MS. (D) Enrichment analysis of the differentially interacting proteins of heterochromatin components is shown on the basis of GO annotation. (E) Immunofluorescence detection of HP1 α foci in WT and FBXO42 KO cells. Scale bars, 10 μ m. (F) HP1 α foci number and percentage of HP1 α foci area were calculated using ImageJ software. (G) WT and FBXO42 KO cells were digested with micrococcal nuclease (MNase) for 3 min, and chromatin relaxation was monitored by the release of nucleosomes. (H) Chromatin association of the SWI/SNF subunits SMARCA2, SMARCA4, and SMARCC2 in WT and FBXO42 KO cells was analyzed using Western blotting after chromatin isolation. ORC2 served as the loading control. (I) WT and FBXO42 KO cells were digested with deoxyribonuclease (DNase I) for 3 min and followed with agarose gel electrophoresis analysis. (J) Chromatin from WT and FBXO42 KO cells was isolated, and DNase I was digested and used as substrate for accessibility assay. (K and L) The heatmap view for ATAC-seq signal intensity at TSSs in WT and FBXO42 KO JURKAT cells. (M) ATAC-seq peaks; H3K4m1, H3K4m3, and H3K27ac ChIP-seq peaks; and DNase-seq peaks downloaded from ENCODE database at MYC locus were analyzed. (A), (B), and (E) to (J), $n = 3$. Quantitative data are presented as means \pm SEM. P values were calculated using two-tailed Student's t tests. * $P < 0.05$ and ** $P < 0.01$.

of the SWI/SNF complex (fig. S4B), which is also highly consistent with the IP-Western blot results (fig. S4A). The chromatin remodeling factor binding pattern of RBPJ in FBXO42 KO cells and RBPJ K175R was very similar (Fig. 5C and fig. S4B).

To determine the overall impact of the FBXO42-RBPJ axis on chromatin remodeling activities, we analyzed the differential interactomes of the key heterochromatin components such as CBX1, CBX3, CBX5, SUV39H1, and TRIM28 between WT and FBXO42 KO cells. Knocking out FBXO42 led to a change in the interaction landscape consisting of these heterochromatin proteins; that is, their interactions with other chromatin remodeling factors—such as BRCA2-interacting transcriptional repressor EMSY (EMSY), Polycomb group RING finger protein 6 (PCGF6), and Polyhomeotic-like protein 2 (PHC2)—were changed (Fig. 5D and fig. S4, C to G), further supporting their potential role in chromatin remodeling regulation. Together, our data indicate that FBXO42 regulates RBPJ chromatin association and transcriptional by promoting RBPJ K175 ubiquitination.

Since these chromatin remodeling complexes are involved in chromatin compaction and relaxation, we wondered whether the FBXO42-RBPJ axis directly modulates chromatin accessibility. The number of heterochromatin protein 1 homolog alpha (HP1 α) foci, which were heterochromatin markers, was significantly increased in FBXO42 KO cells (Fig. 5, E and F). Moreover, the depletion of FBXO42 decreased the level of nucleosome release from chromatin after micrococcal nuclease (MNase) treatment (Fig. 5G) and the chromatin association of SWI/SNF complexes, as exemplified by an analysis of its essential adenosine triphosphatase (ATPase) subunits SWI/SNF-related matrix-associated actin-dependent regulator of chromatin A2 (SMARCA2), SMARCA4, and catalytic core subunit SMARCC2 (Fig. 5H). Deoxyribonuclease I (DNase I) chromatin accessibility analysis indicated less sensitive to DNase I digestion on RBPJ-binding region upon FBXO42 depletion, which is more condensed in its chromatin state (Fig. 5, I and J). Furthermore, assay for transposase-accessible chromatin with high throughput sequencing (ATAC-seq) data showed a global chromatin accessibility change (Fig. 5, K and L) and an effect on leukemia-related transcription factors binding (fig. S4H) after FBXO42 KO. The affected area was mostly related to leukemia promoter and enhancer region as characterized by H3K4me1, H3K4me3, and H3K27ac chromatin immunoprecipitation sequencing (ChIP-seq) and DNase sequencing data from ENCODE database (Fig. 5M and fig. S4I), which was further confirmed by ChIP-quantitative polymerase chain reaction (qPCR) (fig. S4, J and K). Together, FBXO42 increased global chromatin accessibility in an RBPJ-dependent manner, which may act as a modulator of RBPJ's chromatin remodeling function for Notch signaling activation.

FBXO42 plays an essential role in Notch signaling-dependent leukemogenesis

Aberrant activation of the Notch pathway is closely related to the occurrence and progression of T-ALL; however, only a subset of these patients carry *NOTCH* gene mutations (1, 45). Since FBXO42 plays a key role in Notch signaling, we wondered whether FBXO42 contributes to leukemogenesis. Therefore, we tested the protein expression in several T-ALL cell lines and selected the HSB2 and JURKAT cell lines, expressing WT *NOTCH* and relatively high FBXO42 levels, for subsequent studies (Fig. 6A). Knocking out FBXO42 in these two cell lines (Fig. 6B) led to decreased expression of Notch target genes (Fig. 6, C and D). Consistently, FBXO42 KO

leukemia cells showed decreased RBPJ levels in chromatin fraction (Fig. 6, E and F) and reduced levels of chromatin-associated SWI/SNF complex components (Fig. 6G). To further explore the role played by FBXO42 in leukemogenesis, we evaluated the impact of FBXO42 KO on leukemia cell invasion (Fig. 6, H to K), migration (Fig. 6, L to O), and anchorage-independent cell growth (Fig. 6, P to S). The depletion of FBXO42 significantly reduced leukemia cell invasion, migration, and tumorigenesis (Fig. 6, H to S).

To further investigate the extent to which FBXO42 regulation of Notch signaling and leukemogenesis directly depends on RBPJ, we first analyzed the expression of Notch target genes in leukemia cells in the absence of RBPJ (Fig. 6, T and W). Similar to the effect of FBXO42 depletion, the loss of RBPJ in the JURKAT and HSB2 cells decreased the expression of Notch target genes (Fig. 6, U and X). It also repressed sphere formation (fig. S5, A to D) and anchorage-independent growth (fig. S5, E to H), consistent with the FBXO42 KO phenotypes. We further explored the function of FBXO42 in modulating Notch signaling activity in RBPJ-deficient cells. We found that in RBPJ competent cells, the overexpression of FBXO42 led to profound up-regulation of *HES1*, *HES5*, and *c-MYC* expression. However, in RBPJ-deficient cells, the overexpression of FBXO42 induced a mild effect on the expression of *HES1*, *HES5*, and *c-MYC* (Fig. 6, V and Y).

To determine whether the FBXO42 regulation of leukemogenesis is dependent on its ubiquitination activity on RBPJ, we overexpressed WT FBXO42 and the FBXO42 mutant with the F-box deleted in FBXO42 KO cells and determined the rescue effect on cellular phenotypes. Overexpression of WT FBXO42 but not the F-box deletion mutant rescued Notch target gene expression in both FBXO42-deficient HEK293T and leukemia cells (fig. S6, A to C). Moreover, the sphere formation rate (fig. S6, D to G) and anchorage-independent cell growth (fig. S6, H to K) of the leukemia cells were increased when WT FBXO42 but not the F-box-deleted mutant was overexpressed. MLN4924, which abrogated FBXO42-mediated K63-linked polyubiquitination of RBPJ and Notch activation, diminished cell viability (fig. S6L), Notch target gene expression (fig. S6, M and N), and anchorage-independent growth (fig. S6, O to R) of leukemia cells, suggesting that ubiquitination activity was required for FBXO42 regulation of Notch signaling-dependent leukemogenesis. Together, these data demonstrated that FBXO42 played an essential role in Notch signaling and leukemia cell tumorigenesis in a ubiquitination- and RBPJ-dependent manner.

Knocking out FBXO42 inhibits the tumorigenesis of human leukemia cells, mouse xenografts, and leukemia models

To further demonstrate the function of FBXO42 in leukemia pathogenesis, we determined the effect of FBXO42 KO on tumor formation. First, WT and FBXO42 KO JURKAT or HSB2 cells were subcutaneously injected into the left and right flanks of 6-week-old nude mice, respectively, to establish xenograft leukemia models. Tumor formation was monitored for 28 days and measured every 3 days. Both the tumor size and tumor weight in mice injected with the FBXO42 KO JURKAT cells were significantly reduced compared with those in the mice injected with the control JURKAT cells (Fig. 7, A to C). A similar result was obtained in the HSB2-induced xenograft mouse model (Fig. 7, E to G). To evaluate whether the suppressive effect of FBXO42 on tumor formation is related to Notch signaling modulation, tumor tissues derived from different cells were isolated and the expression of classical Notch target genes was detected. Notch target

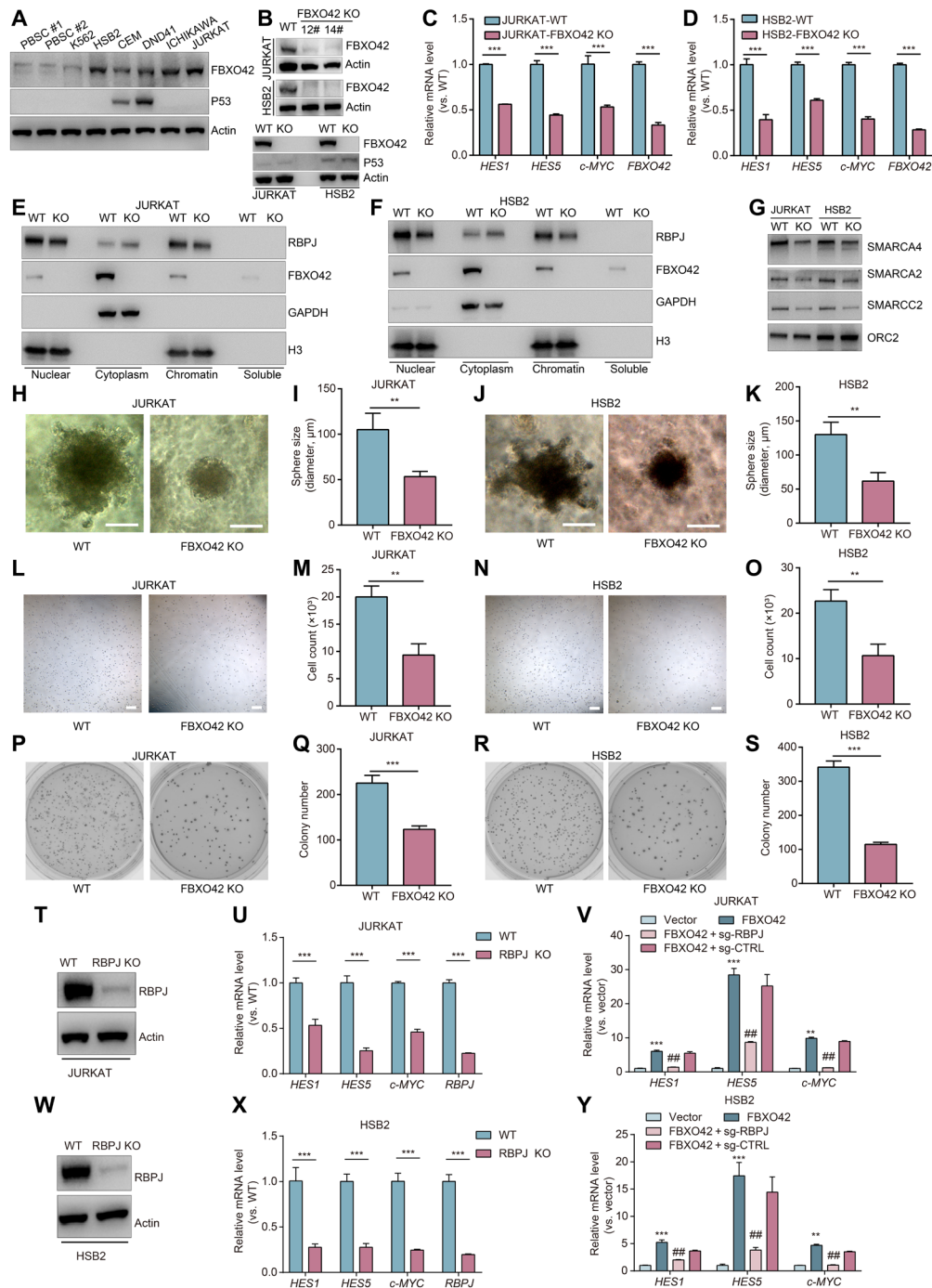


Fig. 6. FBXO42 plays an essential role in Notch signaling-dependent leukemogenesis. (A) Western blots of FBXO42, p53, and actin in various leukemia cell lines. peripheral blood stem cells (PBSC) represents the healthy hematopoietic cell. (B) CRISPR-Cas9-mediated KO of FBXO42 in JURKAT and HSB2 cells was determined by Western blotting (top). Expression of p53 in WT and FBXO42 KO cells was shown (bottom). (C and D) mRNA levels of the Notch target genes in corresponding cells were determined by qPCR. (E and F) Level of RBPJ in different fractions was determined for WT and FBXO42 KO JURKAT (E) and HSB2 (F) cells. GAPDH, glyceraldehyde-3-phosphate dehydrogenase. (G) Chromatin association of the SWI/SNF subunits SMARCA2, SMARCA4, and SMARCC2 in WT and FBXO42 KO leukemia cells. (H to K) Invasion abilities of WT and FBXO42 KO JURKAT (H) and HSB2 (J) cells were measured. Scale bars, 50 μm . The average diameter (I and K) of the spheres was determined. (L to O) Migration abilities of the WT and FBXO42 KO cells detected using a transwell migration assay. Scale bars, 200 μm . Cells that migrated into the lower chamber were counted (M and O). (P to S) Anchorage-independent tumorigenesis abilities of the WT and FBXO42 KO JURKAT (P) and HSB2 (R) cells. The number of colonies in (P) and (R) was counted, respectively (Q and S). (T to Y) FBXO42 functions rely on the presence of RBPJ. The KO efficiency of RBPJ in JURKAT (T) and HSB2 (W) cells was determined by Western blotting. The mRNA levels of Notch target genes under different conditions were determined by qPCR (U, V, X, and Y). (A) to (Y), $n=3$. Quantitative data are presented as means \pm SEM from three independent experiments. P values were calculated using two-tailed Student's t tests or analyzed using a one-way ANOVA for multiple comparisons. ** $P < 0.01$ and *** $P < 0.001$. For data in (V) and (Y), ## $P < 0.01$ versus FBXO42.

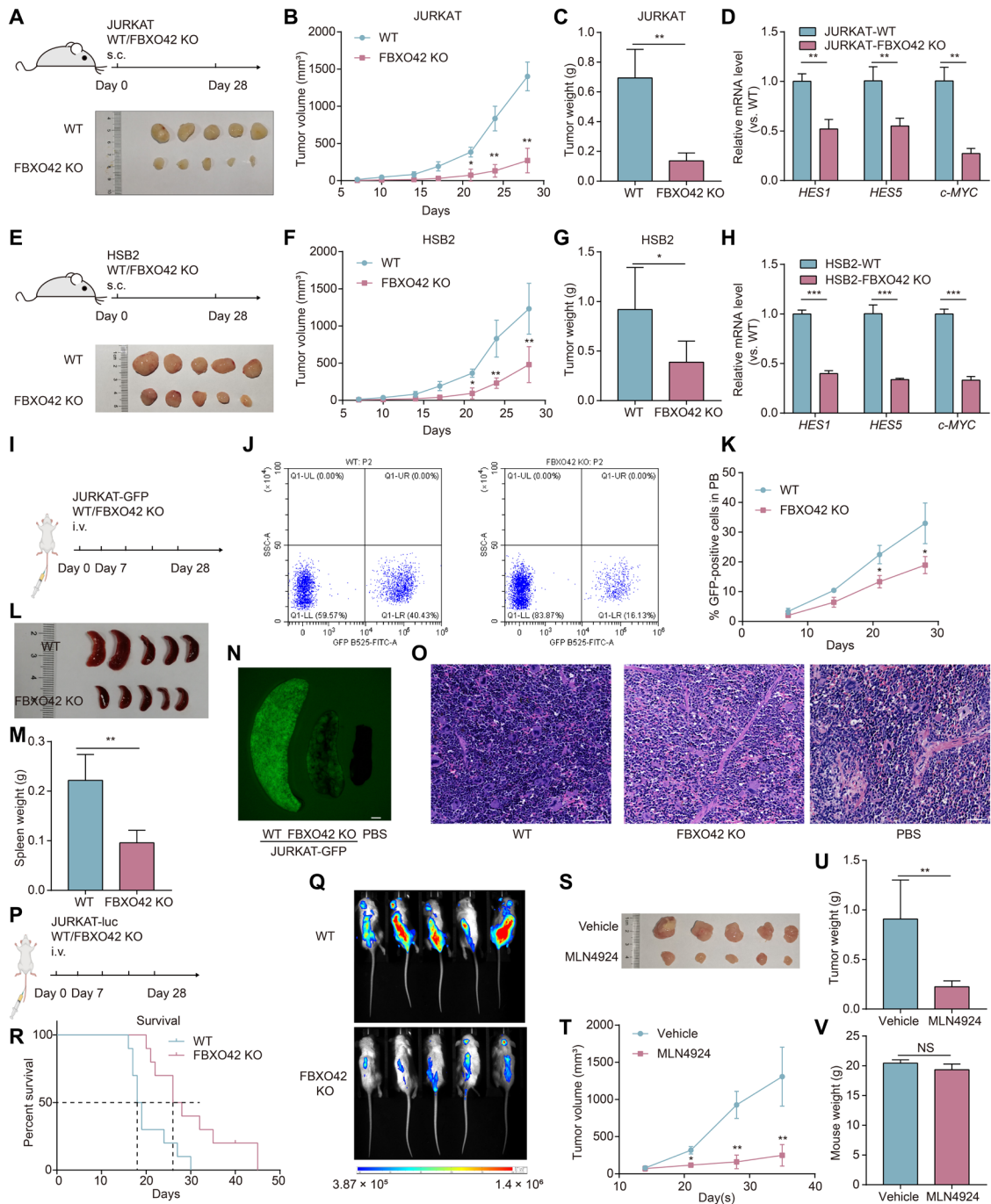


Fig. 7. Genetic and pharmacological targeting of FBXO42 attenuated leukemia progression in vivo. (A to H) Xenograft tumor growth studies were performed with WT or FBXO42 KO JURKAT (A to D) and HSB2 (E to H) cells. Mice were euthanized 4 weeks after tumor cell injection. The tumors were excised, photographed, and weighed. The volumes (B and F) and weights (C and G) of the tumors were measured, respectively. The mRNA levels of Notch target genes in tumors were determined by qPCR, respectively (D and H). s.c., subcutaneous injection. (I to K) In vivo leukemia mouse model was established by injecting WT and FBXO42 KO JURKAT cells carrying GFP into NSG mice intravenously. The percentage of GFP⁺ leukemia cells in peripheral blood (PB) was measured weekly by flow cytometry analysis (I) and summarized (K). Representative flow cytometry dot plots showing the expression of GFP in peripheral blood was shown (J). i.v., intravenous; FITC-A, fluorescein isothiocyanate-A; SSC-A, side scatter area. (L to O) Spleens in mice from different groups were excised, a representative image is shown (L), and the spleen weight was measured (M). Tumor cell invasion was evaluated by measuring the GFP intensity by fluorescence microscopy (N) and hematoxylin and eosin staining (O). Scale bars, 50 μm. (P and Q) NSG mice were transplanted with luciferase-expressing WT and FBXO42 KO JURKAT cells via tail vein injection. Tumor growth in each group was tracked by bioluminescence imaging. (R) Survival analysis of mice in (P). (S to V) Xenograft tumor growth studies were performed with JURKAT cells. Mice bearing JURKAT xenograft were then subcutaneously administered with vehicle or MLN4924 (30 mg/kg) twice daily for 21 days. At the end of the study, the tumors were excised, photographed, and weighed. A macroscopic graph of the tumors is shown (R). The volumes (S) and weights (T) of the tumors as well as the mouse weight (U) were measured. (A) to (O) and (S) to (V), *n* = 5; (P) to (R), *n* = 10. Quantitative data are presented as means ± SEM. *P* values were calculated using two-tailed Student's *t* tests. **P* < 0.05, ***P* < 0.01, and ****P* < 0.001.

gene expression was reduced in the FBXO42 KO cells that formed tumors (Fig. 7, D and H).

We established another mouse model via tail vein injection of leukemia cells to explore the effect of FBXO42 expression on leukemia cell invasion in vivo. Green fluorescent protein (GFP)-labeled WT and FBXO42 KO JURKAT cells were injected into immunodeficient NSG (NOD.Cg-Prkd^{csid} IL2rgtm^{1WJl/SzJ}) mice via the tail vein, and leukemia progression was monitored weekly by measuring the GFP intensity by flow cytometry analysis (Fig. 7I). We observed that knocking out FBXO42 significantly decreased the leukemia burden and progression in peripheral blood (Fig. 7, J and K), as well as splenomegaly (Fig. 7, L and M). We found that leukemia cell infiltration in the spleen and abnormal spleen histology were attenuated in the FBXO42 KO group (Fig. 7, N and O). Moreover, bioluminescence imaging with luciferase containing WT and FBXO42 KO JURKAT cells also confirmed the suppressive effect of FBXO42 on leukemia progression and mouse survival (Fig. 7, P to R). As MLN4924 inhibited leukemia cell viability, we detected its effect in a JURKAT xenograft model. As evidenced by the tumor growth rate, the pharmacological inhibition of FBXO42 activity by MLN4924 reduced the leukemia burden in vivo without inducing obvious toxicity (Fig. 7, S to V). Together, these data suggested that FBXO42 plays a key role in leukemia tumorigenesis both in vitro and in vivo and may be a potential drug target for the interference of Notch-related diseases, especially T-ALL.

DISCUSSION

Increasing evidence, particularly found following the initial discovery of the activating *NOTCH1* mutation in T cell leukemia, indicates that dysregulated Notch signaling plays a pivotal role in tumor initiation and progression (1). Both hyperactivated (1, 2, 6, 46, 47) and hypoactivated (4, 5) Notch signaling led to tumorigenesis, which was consistent with its regulatory role during development, where it either blocks or promotes differentiation in different cellular contexts (48, 49). Similarly, dysregulation of RBPJ expression contributed to tumor progression differentially in different cellular contexts. In glioblastoma (50, 51) and lung cancer (52), RBPJ acts as an oncogene. In many other cancers, RBPJ acts as a tumor suppressor, and its depletion may contribute to the tumorigenesis (17). These complicated outcomes make pharmacologically targeting RBPJ in Notch-related cancers very risky; therefore, we must fully understand the RBPJ functions and regulatory mechanisms in different cellular contexts. A better understanding of the modulation of RBPJ transcriptional activity is essential for clinical transformation.

In this study, we show that FBXO42 interacts with RBPJ. FBXO42 is a component of the SCF E3 ubiquitin ligase complex and is critical for substrate recognition. The SCF complex consists of four subunits, the adaptor protein SKP1, RING finger protein RBX1/2, scaffold protein CULL1, and variable F-box protein that recognizes specific substrates (53). F-box proteins recognize and bind their substrates, which are then targeted for ubiquitination and subsequent degradation in most cases. Nevertheless, the function of FBXO42 is largely unknown, although it has been conserved from fly to human. *Drosophila* FBXO42 promotes synaptonemal complex assembly during female meiosis by down-regulating serine/threonine-protein phosphatase 2A (PP2A)-B56 (54). In humans, it promotes the polyubiquitination of p53, inducing its degradation (29).

In our study, we revealed a role played by the F-box protein FBXO42 in regulating Notch signaling and leukemogenesis. Our

study provided evidence showing that FBXO42 mainly promotes polyubiquitination of RBPJ via the K63 linkage, leading to its functional modulation. FBXO42 inactivation by either genetic KO or pharmacological inhibition attenuated leukemia progression in mouse models. We found that MLN4924, which is currently in phase 1 to 3 clinical trials for the treatment of many types of cancers, modulates FBXO42-promoted K63-linked ubiquitination of RBPJ and subsequently ameliorates leukemia, making it an attractive candidate for treating leukemias with hyperactivated Notch signaling, such as T-ALL, CLL, and DLBCL. Nevertheless, a more specific molecule targeting FBXO42 needs to be identified for use in clinical settings.

SWI/SNF complex components have been reported to be involved in Notch-responsive gene activation, which correlates with increased chromatin accessibility (55, 56); however, the detailed mechanism remains largely unknown. K63 polyubiquitination of several transcription factors/cofactors involved in DNA damage repair has been reported to facilitate chromatin opening and remodeling (57, 58). Our results revealed a central role for FBXO42-promoted K63 polyubiquitination in modulating chromatin accessibility. When ubiquitinated by FBXO42 via K63-linkage, RBPJ acts as a pioneer factor that recruits many chromatin remodelers to increase global chromatin accessibility, subsequently leading to a broad spectrum of transcriptional activation.

In conclusion, our study reveals that the FBXO42-mediated K63-linked polyubiquitination of RBPJ is involved in Notch signaling activation and leukemogenesis. This research extends our knowledge by showing that FBXO42 is an important partner of RBPJ and is critical in the posttranslational modification of RBPJ to trigger its transcriptional activity and pioneer factor function, suggesting that the FBXO42 and RBPJ interaction and RBPJ K175 ubiquitination are potential therapeutic targets for Notch-related diseases.

MATERIALS AND METHODS

Constructs

Genes encoding RBPJ and FBXO42 were amplified from cDNAs by PCR and cloned into a pDONR201 vector (Invitrogen, Carlsbad, CA) as entry clones and subsequently transferred to Gateway compatible destination vectors for the expression of C-terminal S protein tag-2x FLAG tag-Streptavidin binding peptide (SBP) tag (cSFB)- or Myc-tagged fusion proteins. Deletion mutants of FBXO42 and RBPJ were generated by introducing point mutations and were verified by sequencing.

Cell culture and transfection

HEK293T cells were cultured in Dulbecco's modified Eagle's medium (DMEM) supplemented with 10% fetal bovine serum and 1% penicillin/streptomycin (Thermo Fisher Scientific). HSB2 and JURKAT cells were cultured in RPMI 1640 medium supplemented with 10% fetal bovine serum and 1% penicillin/streptomycin in a humidified incubator with 5% CO₂ at 37°C.

To establish HEK293T cells stably expressing cSFB-RBPJ and cSFB-FBXO42, the cells were transfected with the respective plasmids using polyethylenimine (Polysciences) and selected in DMEM supplemented with puromycin (2 µg/ml; Sangon, China) for at least 2 weeks.

For KO experiments, CRISPR constructs were packaged into lentiviruses by cotransfecting them with the packaging plasmids pMD2.G (#12259, Addgene) and psPAX2 (#12260, Addgene) into HEK293T cells. Forty-eight hours after transfection, the cell medium was collected and used to infect HEK293T, HSB2, or JURKAT cells.

The cells were infected twice at an interval of 24 hours to achieve maximal infection efficiency.

Generation of CRISPR-induced KO

A FBXO42 KO HEK293T, JURKAT, and HSB2 cell lines were established by CRISPR-Cas9-mediated genome editing. The target sequences for CRISPR interference were designed using the Benchling tool (2021), ligated into a lentiCRISPR v2 plasmid (#52961, Addgene) (59) at the Bsm BI restriction site, and packaged into lentivirus via cotransfection with the packaging plasmids pMD2.G and psPAX2 in HEK293T cells. HEK293T, JURKAT, and HSB2 cells were infected with lentiCRISPR virus at the desired titer and then selected with puromycin. Individual clones were further expanded, and the loss of target protein expression was confirmed by immunoblotting. The single guide RNA sequences are as follows: *FBXO42* (5'-CGG-CCCTGTCTGCAAACAG-3') and *RBPJ* (5'-AAAGAACAAAT-GGAACGCGA-3').

Western blotting and IP

Cells were washed twice with phosphate-buffered saline (PBS) and dissolved in NETN lysis buffer [20 mM tris-HCl (pH 8.0), 100 mM NaCl, 0.5% NP-40, and 1 mM EDTA] supplemented with protease and phosphatase inhibitors (Sangon, China). Whole-cell lysates were subjected to SDS-polyacrylamide gel electrophoresis (PAGE) and were then immunoblotted with specific antibodies.

For IP, 1×10^7 cells were lysed with NETN buffer on ice for 30 min. The lysates were then incubated with 30 μ l of conjugated S-beads (for SFB-tagged pull-down assay) for 2 hours at 4°C or incubated with antibodies against endogenous proteins for 1 hour at 4°C, followed by the addition of 20 μ l of protein A/G agarose and incubation for 2 hours at 4°C. The immunoprecipitates were washed with lysis buffer three times before immunoblot analysis. The following primary antibodies were used: rabbit anti-RBPJ [5313S, Cell Signaling Technology (CST), RRID:AB_2665555], mouse anti-FBXO42 (TA800283, OriGene, RRID:AB_2625356), THE hemagglutinin (HA) Tag (A01244, GenScript), THE c-Myc Tag (A00704, GenScript), ANTI-FLAG M2 antibody (B3111, Sigma-Aldrich, RRID:AB_2910145), rabbit anti-ubiquitin (AF0306, Beyotime), rabbit anti- β -actin (AC026, ABclonal, RRID:AB_2768234), rabbit anti-LSD1 (YM0422, ImmunoWay), rabbit anti-SMARCA4 (ET1611-85, HUABIO), rabbit anti-SMARCA2 (ER65406, HUABIO), rabbit anti-SMARCC2 (ER62787, HUABIO), and rabbit anti-origin recognition complex subunit 2 (ORC2) (A15697, ABclonal). The following secondary antibodies were used: goat anti-mouse immunoglobulin G (IgG) antibody (H&L) [horseradish peroxidase (HRP)] (A00160, GenScript) and goat anti-rabbit IgG antibody (H&L) (HRP) (A00178, GenScript).

Tandem affinity purification

TAP was performed as previously described (27). Briefly, 1×10^8 HEK293T cells stably expressing cSFB-RBPJ or FBXO42 were lysed in 5 ml of NETN buffer (with protease inhibitors) at 4°C for 30 min, followed by TurboNuclease treatment. The lysate was then incubated with streptavidin-conjugated beads (Thermo Fisher Scientific, Waltham, MA) for 2 hours at 4°C. After washing with NETN buffer, the bound proteins were eluted with NETN buffer containing biotin (2 mg/ml; Sigma-Aldrich, St. Louis, MO) for 2 hours at 4°C. The eluates were then incubated with S-protein beads (EMD Millipore, Burlington, VT) for 4 hours. The beads were washed three times with NETN buffer and subjected to SDS-PAGE, followed

by Coomassie blue staining. The whole band was excised and subjected to in-gel trypsin digestion and MS analysis.

In vivo ubiquitination assay

For the in vivo ubiquitination assay, HEK293T cells were transfected with the indicated plasmids and treated with or without 10 μ M MG132 (S2619, Selleck) for 4 hours before harvest. Whole cells were lysed with NETN buffer containing protease inhibitors. Equal amounts of protein lysates were pulled down with S-protein beads for 4 hours at 4°C. After incubation, the beads were extensively washed three times with NETN buffer, boiled with sample buffer for 20 min, and subjected to SDS-PAGE followed by immunoblotting with antibodies against various proteins as indicated. To detect endogenous RBPJ ubiquitination, the lysate was immunoprecipitated with RBPJ antibody and then immunoblotted with an antibody against ubiquitin.

Quantitative real-time PCR

Total RNA was isolated from cells using TRIzol reagent (Takara), and cDNA synthesis was performed using 1 μ g of total RNA with HiScript III reverse transcriptase (R212-02, Vazyme). The levels of mRNA for the specific genes were quantified by SYBR Green qPCR according to the manufacturer's guidance on a Jena qTOWER³G qPCR System. The relative mRNA levels were determined using the comparative C_t method with actin as the reference gene following the formula $2^{-\Delta\Delta C_t}$. The primers used are listed as follows: *HES1*, 5'-CCTGTCATCCCCGTCTACAC-3' (forward) and 5'-CACATGGAGTCCGCCGTAA-3' (reverse); *HES5*, 5'-CGCATCAACAGCAGCATCGAG-3' (forward) and 5'-GACGAAGGCTTTGCTGTGCT-3' (reverse); *c-MYC*, 5'-GGCTCCTGGCAAAGGTCA-3' (forward) and 5'-CTGCGTAGTTGTGCTGATGT-3' (reverse); *Actin*, 5'-TTGCCGACAGGATGCAGAAGGA-3' (forward) and 5'-AGGTGGA-CAGCGAGGCCAGGAT-3' (reverse).

Luciferase reporter assay

Luciferase reporter constructs containing the *HES1* and *HES5* promoters and 8 \times RBPJ-binding sites were generated by inserting the *HES1* and *HES5* promoters and the 8 \times RBPJ binding site sequence into the pGL3 basic luciferase vector upstream of the firefly luciferase gene. For the luciferase assay, HEK293T cells were plated at 50% confluency in 24-well plates and grown overnight. The firefly luciferase reporter construct and the *Renilla* control reporter were cotransfected into the cells at a molar ratio of 10:1. After 24 hours of culture, the luciferase activity was assayed with the Dual Luciferase Assay Kit (11402ES60, YEASEN) with normalization to *Renilla* activity.

Cell Counting Kit-8 assay

The cell viability was measured by Cell Counting Kit-8 (CCK-8) assay according to the manufacturer's guidance (C0005, TargetMol). JURKAT and HSB2 cells were incubated with vehicle or MLN4924 (HY-10484, MedChemExpress) at different concentrations as indicated for 36 hours. Then, cells were handled by CCK-8 reagent and continued to incubate for another 4 hours. The absorbance was detected at 450 nm, and the related cell viability was measured.

Immunofluorescence

Cells were seeded in a cell culture dish, fixed with 4% paraformaldehyde at room temperature for 10 min, permeabilized 10 min with 0.1% Triton X-100, washed with PBS, and blocked in 5% bovine serum albumin in PBS for 30 min before labeling with anti-HP1 α primary

antibody (ab109028, Abcam, RRID:AB_10858495) at room temperature for 1 hour. After incubation, cells were washed with PBS twice, stained with goat anti-rabbit Alexa Fluor 488-labeled IgG (ab150077, Abcam, RRID:AB_2630356) at room temperature for 1 hour, and subjected to 4',6-diamidino-2-phenylindole (DAPI) staining (4083S, CST). Coverslips were mounted using FluorSave reagent (345789, Millipore). The cells were viewed using an Olympus FV3000 Microscope Imaging System (Olympus, Japan).

Chromatin fractionation

To isolate cytoplasm and chromatin fractions, WT and FBXO42 KO HEK293T or leukemia cells were harvested and fractionated as previously described (27, 60) with slight modifications. Briefly, cells were resuspended in cold buffer A [10 mM Hepes (pH 7.9), 10 mM KCl, 1.5 mM MgCl₂, 0.34 M sucrose, 10% glycerol, 1 mM dithiothreitol (DTT), and 0.1% Triton X-100] containing protease inhibitors for 5 min at 4°C. Lysates were centrifuged at 1500g for 5 min, the supernatant was further clarified by high-speed centrifugation (13,000g for 10 min at 4°C) to remove cell debris and insoluble aggregates and collected as the cytoplasm fraction. The nuclei were washed once with buffer A without 0.1% Triton X-100 and then lysed in buffer B (3 mM EDTA, 0.2 mM EGTA, and 1 mM DTT) containing protease inhibitors for 10 min at 4°C. The soluble nuclear proteins were separated from chromatin by centrifugation (2000g for 5 min). Isolated chromatin-enriched pellets were washed once with buffer B and spun down at high speed (13,000g for 1 min), followed by lysing in 2× Laemmli sample buffer. The samples were then subjected to SDS-PAGE, followed by immunoblotting with antibodies against various proteins as indicated.

CUT&Tag assay and sequencing

CUT&Tag assay was performed as previously described (61). Briefly, 100,000 WT and FBXO42 KO cells were collected and lysed according to the manufacturer's guidance (catalog no. 12597, YEASEN). Cell lysates were incubated at room temperature with concanavalin A-coated magnetic beads for 1 hour and then with the primary antibody against RBPJ (1:50; ab25949, Abcam) for 2 hours, with secondary antibodies for 1 hour, and with pA/G-Tn5 adapter complex for 1 hour. The tagmentation takes 1 hour, and DNAs were extracted using a DNA purification kit. Libraries were prepared using the Hieff NGS Tagment Index Kit for Illumina (96 index) (catalog no. 12610, YEASEN) and pooled together for paired-end 150-base pair (bp) sequencing on a NovaSeq (Novogene). Raw fastq files were trimmed using Trim Galore and aligned to the human genome (hg38) using Bowtie2. Reads were sorted and converted to BAM format, and data track visualization occurred using Integrative Genomics Viewer (IGV). Final data analysis and visualization were performed using in-house R scripts.

MNase and DNase sensitivity assays

MNase and DNase sensitivity assays were performed as described previously (62) with some modifications. Briefly, cell pellets were lysed in buffer A [10 mM Hepes (pH 7.9), 10 mM KCl, 1.5 mM MgCl₂, 0.34 M sucrose, 10% glycerol, 1 mM DTT, and 0.1% Triton X-100] for 10 min on ice. The nuclei were pelleted and digested with MNase (10 U/ml; 2910A, Takara) in digestion buffer [10 mM tris-HCl (pH 7.5), 1 mM NaCl, 3 mM MgCl₂, and 1 mM CaCl₂] for 3 min at 37°C or digested with DNase [M0303S, New England Biolabs (NEB)] for 5 min at 37°C. Treated nuclei were lysed, followed

by ribonuclease A (RNase A) and proteinase K digestion. Genomic DNA was purified using a DNA purification kit (DC301-01, Vazyme) and separated by 1.2% agarose gel electrophoresis. DNA bands were visualized under a Gel Doc XR+ System (Bio-Rad).

DNase I chromatin accessibility analysis

Chromatin accessibility was analyzed as previously reported (63, 64). Briefly, chromatin was isolated in a buffer containing 10 mM tris-HCl (pH 7.5), 5 mM MgCl₂, 1 mM CaCl₂, 10 mM KCl, 300 mM sucrose, and 0.1% Triton X-100 for 5 min on ice, washed, and re-suspended with the same buffer without detergent. The one-third chromatin was then digested with DNase I (NEB) at 3 U per 100 μl for 7 min at room temperature, and the other one-third was treated identically without DNase I (untreated control for normalization). Reactions were stopped by adding 10 mM EDTA and 2 mM EGTA and incubated at 65°C for 10 min. DNA was briefly sonicated and treated with RNase (50 μg/ml; Sigma-Aldrich) for 30 min at 37°C followed by proteinase K (250 μg/ml; Sigma-Aldrich) for 2 hours at 42°C. DNA was purified and analyzed using Jena qTOWER³G System. qPCR results were analyzed according to the formula $100/2^{Ct(DNase\ I) - Ct(no\ DNase\ I)}$ for normalization to input DNA (no DNase I treatment).

ATAC-seq library preparation and data analysis

ATAC-seq library processing was performed according to the manufacturer's protocol (N248, Novoprotein). Briefly, 50,000 viable cells were resuspended and nuclei were isolated. The transposition was performed using Tn5 transposase, which was followed by adaptor ligation and PCR amplification. Libraries were sequenced with 150-bp paired-end on NovaSeq. All paired-end reads were first subjected to adaptor trimming using Cutadapt (v1.18). The clipped reads were aligned to the human genome (hg38) using bowtie2 (v2.3.3.1). Peaks were called for each sample using MACS2 (v2.1.1.20160309). ATAC-seq signal was visualized in IGV (v2.5.3) and analyzed using deepTools (v3.3.0).

Global MS-based analysis of protein ubiquitination

Global protein ubiquitination analysis was performed according to the manufacturer's guidance (5562, CST). Briefly, the cell lysis was prepared in urea buffer, followed by reduction, alkylation, and digestion with trypsin overnight. Then, the peptides were used for immunoaffinity purification using Remnant Motif (K-ε-GG) and MS detection.

Chromatin IP

ChIP assay was performed on the basis of the previously described protocol (65). Cells were cross-linked with 1% formaldehyde for 10 min and quenched by 125 mM glycine for 5 min at room temperature with gentle shaking. After rinsing with cold PBS twice, cells were collected in PBS supplemented with protease inhibitors, centrifuged, and lysed in ice-cold lysis buffer [1% SDS, 5 mM EDTA, and 50 mM tris-HCl (pH 8.1)] supplemented with protease inhibitor for 10 min. The cell lysate was sonicated using a Bioruptor sonicator (Diagenode) to break DNA into ~500-bp fragments for ChIP-qPCR. Soluble chromatin was diluted in dilution buffer [1% Triton X-100, 2 mM EDTA, 150 mM NaCl, and 20 mM tris-HCl (pH 8.1)], and 4 μg of ChIP-grade antibody was added and incubated at 4°C for 2 hours with gentle shaking. Protein A/G beads slurry (50 μl; 16-663, Millipore) was added and incubated for 1 hour at

4°C. The beads were then washed in the following buffers for 10 min each at 4°C: buffer I [0.1% SDS, 1% Triton X-100, 2 mM EDTA, 150 mM NaCl, and 20 mM tris-HCl (pH 8.1)], buffer II [0.1% SDS, 1% Triton X-100, 2 mM EDTA, 500 mM NaCl, and 20 mM tris-HCl (pH 8.1)], buffer III [0.25 mM LiCl, 1% NP-40, 1% deoxycholate, 1 mM EDTA, 10 mM tris-HCl (pH 8.1)], and Tris-EDTA buffer [10 mM Tris, 1 mM EDTA, (pH 8.0)] (two times). To elude the DNA, beads were incubated in elution buffer (1% SDS and 0.1 M NaHCO₃) at room temperature with aggressive shaking for 15 min. The supernatant was then collected and incubated at 65°C overnight to reverse cross-link the DNA. DNA purification kit (DC301-01, Vazyme) was used for purifying the DNA for the subsequent qPCR. The following antibodies were used in ChIP: anti-H3K4me3 (ab8580, Abcam, RRID:AB_306649), anti-H3K27ac (ab177178, Abcam, RRID:AB_2828007), and anti-IgG (3900S, CST, RRID:AB_1550038). ChIP-qPCR experiments were done in triplicate, and the results were normalized to the input DNA.

Mouse model

All animal experiments were performed in accordance with a protocol approved by the Institutional Animal Care and Use Committee of Westlake University (AP#20-023-LX). Five to 10 mice were randomly assigned to each group of each study. WT and FBXO42 KO HSB2 and JURKAT cells (5×10^6) were resuspended separately in 100 μ l of Matrigel (356237, Corning) diluted with PBS at a 1:1 ratio and subcutaneously injected into the left and right flanks, respectively, of anesthetized 6- to 8-week-old female BALB/c nude mice (Shanghai Laboratory Animals Center). Starting on day 7, tumor formation was observed biweekly. The mice were euthanized after 4 weeks of injection, and the tumors were excised, photographed, and weighed.

For the invasion assay, a leukemia model was established with NSG mice (Charles River Laboratories). WT and FBXO42 KO JURKAT-GFP reporter cells (5×10^6) were resuspended in 100 μ l of PBS and intravenously injected into 6- to 8-week-old female NSG mice via the tail vein. Starting on day 7, peripheral blood leukemia cells were analyzed by detecting GFP levels with flow cytometry. At the end of the study, the mice were euthanized, and the spleen tissues were excised, photographed, fixed in 4% paraformaldehyde, paraffin-embedded, and stained with hematoxylin and eosin.

For the evaluation of MLN4924 efficacy *in vivo*, 6- to 8-week-old female BALB/c nude mice were inoculated with 5×10^6 JURKAT cells subcutaneously in the right flank, and the tumor growth was monitored with caliper measurements. When the tumor was visible, the mice were subcutaneously dosed with vehicle or MLN4924 (30 mg/kg, twice daily) for 21 days, and the tumor growth was then recorded.

In vivo bioluminescence imaging

To monitor tumor growth in living animals, JURKAT cells used for the animal studies were transduced with firefly luciferase through lentiviral infection. Then, the cells were infected with lentiCRISPR virus to knock out FBXO42, and these infected cells were intravenously engrafted into 6- to 8-week-old female NSG mice. For the imaging analysis, the animals were intraperitoneally administered with D-luciferin (150 mg/kg; 40902ES01, YEASEN) and anesthetized with isoflurane. Tumor luciferase images were captured with an IVIS imaging system (Biospace Imager Optima).

Histological analysis

Spleen tissues collected from different groups of mice were fixed in 4% paraformaldehyde and immersed in fixative for 24 hours. After

embedding into paraffin, sections (4 μ m) were prepared and placed on poly-L-lysine-coated slides. Morphological changes were analyzed by hematoxylin and eosin staining.

Flow cytometry analysis

Peripheral blood was collected from NSG mice, and red blood cells were removed by RBC lysis (C3702, Beyotime). After washing the cells three times with PBS, GFP intensity was analyzed with a CytoFLEX flow cytometer and CytExpert software according to the manufacturer's instructions.

Statistical analysis

All Western blotting, immunofluorescence, and real-time-qPCR (RT-qPCR) data were obtained from at least three repeated experiments. All data were included. The data were analyzed using Prism 7.0 software (GraphPad, USA) and are presented as the mean values (\pm SEM). Statistical significance between two groups was determined by unpaired two-tailed Student's *t* test. Multiple group comparisons were performed by one-way analysis of variance (ANOVA). *P* values of <0.05 [indicated with an asterisk (*)] were considered significant.

SUPPLEMENTARY MATERIALS

Supplementary material for this article is available at <https://science.org/doi/10.1126/sciadv.abq4831>

[View/request a protocol for this paper from Bio-protocol.](#)

REFERENCES AND NOTES

1. A. P. Weng, A. A. Ferrando, W. Lee, J. P. Morris IV, L. B. Silverman, C. Sanchez-Irizarry, S. C. Blacklow, A. T. Look, J. C. Aster, Activating mutations of *NOTCH1* in human T cell acute lymphoblastic leukemia. *Science* **306**, 269–271 (2004).
2. X. S. Puente, S. Beà, R. Valdés-Mas, N. Villamor, J. Gutiérrez-Abril, J. I. Martín-Subero, M. Munar, C. Rubio-Pérez, P. Jares, M. Aymerich, T. Baumann, R. Beekman, L. Belver, A. Carrio, G. Castellano, G. Clot, E. Colado, D. Colomer, D. Costa, J. Delgado, A. Enjuanes, X. Estivill, A. A. Ferrando, J. L. Gelpi, B. González, S. González, M. González, M. Gut, J. M. Hernández-Rivas, M. López-Guerra, D. Martín-García, A. Navarro, P. Nicolás, M. Orozco, Á. R. Payer, M. Pinyol, D. G. Pisano, D. A. Puente, A. C. Queirós, V. Quesada, C. M. Romeo-Casabona, C. Royo, R. Royo, M. Rozman, N. Russiñol, I. Salaverria, K. Stamatopoulos, H. G. Stunnenberg, D. Tamborero, M. J. Terol, A. Valencia, N. López-Bigas, D. Torrents, I. Gut, A. López-Guillermo, C. López-Otín, E. Campo, Non-coding recurrent mutations in chronic lymphocytic leukaemia. *Nature* **526**, 519–524 (2015).
3. K. Karube, A. Enjuanes, I. Dlouhy, P. Jares, D. Martín-García, F. Nadeu, G. R. Ordóñez, J. Rovira, G. Clot, C. Royo, A. Navarro, B. Gonzalez-Farre, A. Vaghefi, G. Castellano, C. Rubio-Perez, D. Tamborero, J. Briones, A. Salar, J. M. Sancho, S. Mercadal, E. Gonzalez-Barca, L. Escoda, H. Miyoshi, K. Ohshima, K. Miyawaki, K. Kato, K. Akashi, A. Mozos, L. Colomo, M. Alcoceba, A. Valera, A. Carrió, D. Costa, N. Lopez-Bigas, R. Schmitz, L. M. Staudt, I. Salaverria, A. López-Guillermo, E. Campo, Integrating genomic alterations in diffuse large B-cell lymphoma identifies new relevant pathways and potential therapeutic targets. *Leukemia* **32**, 675–684 (2018).
4. N. Agrawal, M. J. Frederick, C. R. Pickering, C. Bettgowda, K. Chang, R. J. Li, C. Fakhry, T.-X. Xie, J. Zhang, J. Wang, N. Zhang, A. K. El-Naggar, S. A. Jasser, J. N. Weinstein, L. Treviño, J. A. Drummond, D. M. Muzny, Y. Wu, L. D. Wood, R. H. Hruban, W. H. Westra, W. M. Koch, J. A. Califano, R. A. Gibbs, D. Sidransky, B. Vogelstein, V. E. Velculescu, N. Papadopoulos, D. A. Wheeler, K. W. Kinzler, J. N. Myers, Exome sequencing of head and neck squamous cell carcinoma reveals inactivating mutations in *NOTCH1*. *Science* **333**, 1154–1157 (2011).
5. N. Stransky, A. M. Egloff, A. D. Tward, A. D. Kostic, K. Cibulskis, A. Sivachenko, G. V. Kryukov, M. S. Lawrence, C. Sougnez, A. McKenna, E. Shefler, A. H. Ramos, P. Stojanov, S. L. Carter, D. Voet, M. L. Cortés, D. Auclair, M. F. Berger, G. Saksena, C. Guiducci, R. C. Onofrio, M. Parkin, M. Romkes, J. L. Weissfeld, R. R. Seethala, L. Wang, C. Rangel-Escareño, J. C. Fernandez-Lopez, A. Hidalgo-Miranda, J. Melendez-Zajgla, W. Winkler, K. Ardlie, S. B. Gabriel, M. Meyerson, E. S. Lander, G. Getz, T. R. Golub, L. A. Garraway, J. R. Grandis, The mutational landscape of head and neck squamous cell carcinoma. *Science* **333**, 1157–1160 (2011).
6. D. R. Robinson, S. Kalyana-Sundaram, Y.-M. Wu, S. Shankar, X. Cao, B. Ateeq, I. A. Asangani, M. Iyer, C. A. Maher, C. S. Grasso, R. J. Lonigro, M. Quist, J. Siddiqui, R. Mehra, X. Jing, T. J. Giordano, M. S. Sabel, C. G. Kleer, N. Palanisamy, R. Natrajan,

- M. B. Lambros, J. S. Reis-Filho, C. Kumar-Sinha, A. M. Chinnaiyan, Functionally recurrent rearrangements of the MAST kinase and Notch gene families in breast cancer. *Nat. Med.* **17**, 1646–1651 (2011).
- S. Stylianou, R. B. Clarke, K. Brennan, Aberrant activation of notch signaling in human breast cancer. *Cancer Res.* **66**, 1517–1525 (2006).
 - Y. Wu, C. Cain-Hom, L. Choy, T. J. Hagenbeek, G. P. de Leon, Y. Chen, D. Finkle, R. Venook, X. Wu, J. Ridgway, D. Schahin-Reed, G. J. Dow, A. Shelton, S. Stawicki, R. J. Watts, J. Zhang, R. Choy, P. Howard, L. Kadyk, M. Yan, J. Zha, C. A. Callahan, S. G. Hymowitz, C. W. Siebel, Therapeutic antibody targeting of individual Notch receptors. *Nature* **464**, 1052–1057 (2010).
 - M. López-Guerra, S. Xargay-Torrent, P. Fuentes, J. Roldán, B. González-Farré, L. Rosich, E. Silkenstedt, M. J. García-León, E. Lee-Vergés, N. Giménez, A. Giró, M. Aymerich, N. Villamor, J. Delgado, A. López-Guillermo, X. S. Puente, E. Campo, M. L. Toribio, D. Colomer, Specific NOTCH1 antibody targets DLL4-induced proliferation, migration, and angiogenesis in NOTCH1-mutated CLL cells. *Oncogene* **39**, 1185–1197 (2020).
 - P. J. Real, V. Tosello, T. Palomero, M. Castillo, E. Hernandez, E. de Stanchina, M. L. Sulis, K. Barnes, C. Sawai, I. Homminga, J. Meijerink, I. Aifantis, G. Basso, C. Cordon-Cardo, W. Ai, A. Ferrando, γ -Secretase inhibitors reverse glucocorticoid resistance in T cell acute lymphoblastic leukemia. *Nat. Med.* **15**, 50–58 (2009).
 - J. H. van Es, M. E. van Gijn, O. Riccio, M. van den Born, M. Vooijs, H. Begthel, M. Cozijnsen, S. Robine, D. J. Winton, F. Radtke, H. Clevers, Notch/ γ -secretase inhibition turns proliferative cells in intestinal crypts and adenomas into goblet cells. *Nature* **435**, 959–963 (2005).
 - H. Y. Kao, P. Ordentlich, N. Koyano-Nakagawa, Z. Tang, M. Downes, C. R. Kintner, R. M. Evans, T. Kadesch, A histone deacetylase corepressor complex regulates the Notch signal transduction pathway. *Genes Dev.* **12**, 2269–2277 (1998).
 - P. Mulligan, F. Yang, L. di Stefano, J. Y. Ji, J. Ouyang, J. L. Nishikawa, D. Toiber, M. Kulkarni, Q. Wang, S. H. Najafi-Shoushtari, R. Mostoslavsky, S. P. Gygi, G. Gill, N. J. Dyson, A. M. Näär, A SIRT1-LSD1 corepressor complex regulates Notch target gene expression and development. *Mol. Cell* **42**, 689–699 (2011).
 - T. Xu, S. S. Park, B. D. Giaimo, D. Hall, F. Ferrante, D. M. Ho, K. Hori, L. Anhezini, I. Ertl, M. Bartkuhn, H. Zhang, E. Milon, K. Ha, K. P. Conlon, R. Kuick, B. Govindarajoo, Y. Zhang, Y. Sun, Y. Dou, V. Basrur, K. S. J. Elenitoba-Johnson, A. I. Nesvizhskii, J. Ceron, C.-Y. Lee, T. Borggrefe, R. A. Kovall, J.-F. Rual, RBPJ/CBF1 interacts with L3MBTL3/MBT1 to promote repression of Notch signaling via histone demethylase KDM1A/LSD1. *EMBO J.* **36**, 3232–3249 (2017).
 - H. Kurooka, T. Honjo, Functional interaction between the mouse notch1 intracellular region and histone acetyltransferases PCAF and GCN5. *J. Biol. Chem.* **275**, 17211–17220 (2000).
 - E. Vasyutina, D. C. Lenhard, H. Wende, B. Erdmann, J. A. Epstein, C. Birchmeier, RBP-J (*Rbpsiuh*) is essential to maintain muscle progenitor cells and to generate satellite cells. *Proc. Natl. Acad. Sci. U.S.A.* **104**, 4443–4448 (2007).
 - I. Kulic, G. Robertson, L. Chang, J. H. E. Baker, W. W. Lockwood, W. Mok, M. Fuller, M. Fournier, N. Wong, V. Chou, M. D. Robinson, H.-J. Chun, B. Gilks, B. Kempkes, T. A. Thomson, M. Hirst, A. I. Minchinton, W. L. Lam, S. Jones, M. Marra, A. Karsan, Loss of the Notch effector RBPJ promotes tumorigenesis. *J. Exp. Med.* **212**, 37–52 (2015).
 - Y. Nam, P. Sliz, W. S. Pear, J. C. Aster, S. C. Blacklow, Cooperative assembly of higher-order Notch complexes functions as a switch to induce transcription. *Proc. Natl. Acad. Sci. U.S.A.* **104**, 2103–2108 (2007).
 - M. R. Hass, H.-H. Liow, X. Chen, A. Sharma, Y. U. Inoue, T. Inoue, A. Reeb, A. Martens, M. Fulbright, S. Raju, M. Stevens, S. Boyle, J.-S. Park, M. T. Weirauch, M. R. Brent, R. Kopan, SpDamID: Marking DNA bound by protein complexes identifies notch-dimer responsive enhancers. *Mol. Cell* **59**, 685–697 (2015).
 - H. Liu, A. W. S. Chi, K. L. Arnett, M. Y. Chiang, L. Xu, O. Shestova, H. Wang, Y.-M. Li, A. Bhandoola, J. C. Aster, S. C. Blacklow, W. S. Pear, Notch dimerization is required for leukemogenesis and T-cell development. *Genes Dev.* **24**, 2395–2407 (2010).
 - R. Torella, J. Li, E. Kinrade, G. Cerda-Moya, A. N. Contreras, R. Foy, R. Stojnic, R. C. Glen, R. A. Kovall, B. Adryan, S. J. Bray, A combination of computational and experimental approaches identifies DNA sequence constraints associated with target site binding specificity of the transcription factor CSL. *Nucleic Acids Res.* **42**, 10550–10563 (2014).
 - R. Liefke, F. Oswald, C. Alvarado, D. Ferres-Marco, G. Mittler, P. Rodriguez, M. Dominguez, T. Borggrefe, Histone demethylase KDM5A is an integral part of the core Notch-RBP-J repressor complex. *Genes Dev.* **24**, 590–601 (2010).
 - F. Oswald, P. Rodriguez, B. D. Giaimo, Z. A. Antonello, L. Mira, G. Mittler, V. N. Thiel, K. J. Collins, N. Tabaja, W. Cizelsky, M. Rothe, S. J. Kühl, M. Kühl, F. Ferrante, K. Hein, R. A. Kovall, M. Dominguez, T. Borggrefe, A phospho-dependent mechanism involving NCoR and KMT2D controls a permissive chromatin state at Notch target genes. *Nucleic Acids Res.* **44**, 4703–4720 (2016).
 - A.-S. Geimer Le Lay, A. Oravec, J. Mastio, C. Jung, P. Marchal, C. Ebel, D. Dembélé, B. Jost, L. A. Gras, C. Thibault, T. Borggrefe, P. Kastner, S. Chan, The tumor suppressor Ikaros shapes the repertoire of notch target genes in T cells. *Sci. Signal* **7**, ra28 (2014).
 - S. Chari, S. Winandy, Ikaros regulates Notch target gene expression in developing thymocytes. *J. Immunol.* **181**, 6265–6274 (2008).
 - T. Geiger, A. Wehner, C. Schaab, J. Cox, M. Mann, Comparative proteomic analysis of eleven common cell lines reveals ubiquitous but varying expression of most proteins. *Mol. Cell Proteomics* **11**, M111 014050 (2012).
 - W. Bian, M. Tang, H. Jiang, W. Xu, W. Hao, Y. Sui, Y. Hou, L. Nie, H. Zhang, C. Wang, N. Li, J. Wang, J. Qin, L. Wu, X. Ma, J. Chen, W. Wang, X. Li, Low-density-lipoprotein-receptor-related protein 1 mediates Notch pathway activation. *Dev. Cell* **56**, 2902–2919 e8 (2021).
 - D. S. Chandrashekar, S. K. Karthikeyan, P. K. Korla, H. Patel, A. R. Shovon, M. Athar, G. J. Netto, Z. S. Qin, S. Kumar, U. Manne, C. J. Creighton, S. Varambally, UALCAN: An update to the integrated cancer data analysis platform. *Neoplasia* **25**, 18–27 (2022).
 - L. Sun, L. Shi, W. Li, W. Yu, J. Liang, H. Zhang, X. Yang, Y. Wang, R. Li, X. Yao, X. Yi, Y. Shang, JFK, a Kelch domain-containing F-box protein, links the SCF complex to p53 regulation. *Proc. Natl. Acad. Sci. U.S.A.* **106**, 10195–10200 (2009).
 - S. Lyapina, G. Cope, A. Shevchenko, G. Serino, T. Tsuge, C. Zhou, D. A. Wolf, N. Wei, A. Shevchenko, R. J. Deshaies, Promotion of NEDD8-CUL1 conjugate cleavage by COP9 signalosome. *Science* **292**, 1382–1385 (2001).
 - R. Groisman, J. Polanowska, I. Kuraoka, J.-i. Sawada, M. Saijo, R. Drapkin, A. F. Kisselev, K. Tanaka, Y. Nakatani, The ubiquitin ligase activity in the DDB2 and CSA complexes is differentially regulated by the COP9 signalosome in response to DNA damage. *Cell* **113**, 357–367 (2003).
 - T. A. Soucy, P. G. Smith, M. A. Milhollen, A. J. Berger, J. M. Gavin, S. Adhikari, J. E. Brownell, K. E. Burke, D. P. Cardin, S. Critchley, C. A. Cullis, A. Doucette, J. J. Garnsey, J. L. Gaulin, R. E. Gershman, A. R. Lublinsky, A. McDonald, H. Mizutani, U. Narayanan, E. J. Olhava, S. Peluso, M. Rezaei, M. D. Sintchak, T. Talreja, M. P. Thomas, T. Traore, S. Vyskocil, G. S. Weatherhead, J. Yu, J. Zhang, L. R. Dick, C. F. Claiborne, M. Rolfe, J. B. Bolen, S. P. Langston, An inhibitor of NEDD8-activating enzyme as a new approach to treat cancer. *Nature* **458**, 732–736 (2009).
 - T. A. Soucy, P. G. Smith, M. Rolfe, Targeting NEDD8-activated cullin-RING ligases for the treatment of cancer. *Clin. Cancer Res.* **15**, 3912–3916 (2009).
 - C. M. Pickart, D. Fushman, Polyubiquitin chains: Polymeric protein signals. *Curr. Opin. Chem. Biol.* **8**, 610–616 (2004).
 - R. Kopan, M. X. G. Ilagan, The canonical Notch signaling pathway: Unfolding the activation mechanism. *Cell* **137**, 216–233 (2009).
 - K. Tanigaki, T. Honjo, Two opposing roles of RBP-J in Notch signaling. *Curr. Top. Dev. Biol.* **92**, 231–252 (2010).
 - T. Wang, Z. Huang, N. Huang, Y. Peng, M. Gao, X. Wang, W. Feng, Inhibition of KPNB1 inhibits proliferation and promotes apoptosis of chronic myeloid leukemia cells through regulation of E2F1. *Oncotargets Ther.* **12**, 10455–10467 (2019).
 - L. Harder, G. Eschenburg, A. Zech, N. Kriebitzsch, B. Otto, T. Streichert, A. S. Behlich, K. Dierck, B. Klingler, A. Hansen, M. Stanulla, M. Zimmermann, E. Krenmer, C. Stocking, M. A. Horstmann, Aberrant ZNF423 impedes B cell differentiation and is linked to adverse outcome of ETV6-RUNX1 negative B precursor acute lymphoblastic leukemia. *J. Exp. Med.* **210**, 2289–2304 (2013).
 - E. C. Page, S. L. Heatley, L. N. Eadie, B. J. McClure, C. E. de Bock, S. Omari, D. T. Yeung, T. P. Hughes, P. Q. Thomas, D. L. White, *HMG1* plays a significant role in *CLRF2* driven Down Syndrome leukemia and provides a potential therapeutic target in this high-risk cohort. *Oncogene* **41**, 797–808 (2022).
 - S. J. Erkeland, M. Valkhof, C. Heijmans-Antonissen, R. Delwel, P. J. M. Valk, M. H. A. Hermans, I. P. Touw, The gene encoding the transcriptional regulator Yin Yang 1 (YY1) is a myeloid transforming gene interfering with neutrophilic differentiation. *Blood* **101**, 1111–1117 (2003).
 - X. Chen, S. Yang, J. Zeng, M. Chen, miR-1271-5p inhibits cell proliferation and induces apoptosis in acute myeloid leukemia by targeting ZIC2. *Mol. Med. Rep.* **19**, 508–514 (2019).
 - B. Zhang, K. J. Chambers, D. V. Faller, S. Wang, Reprogramming of the SWI/SNF complex for co-activation or co-repression in prohibitin-mediated estrogen receptor regulation. *Oncogene* **26**, 7153–7157 (2007).
 - B. B. Liao, C. Sievers, L. K. Donohue, S. M. Gillespie, W. A. Flavahan, T. E. Miller, A. S. Venteicher, C. H. Herbert, C. D. Carey, S. J. Rodig, S. J. Shareef, F. J. Najm, P. van Galen, H. Wakimoto, D. P. Cahill, J. N. Rich, J. C. Aster, M. L. Suvà, A. P. Patel, B. E. Bernstein, Adaptive chromatin remodeling drives glioblastoma stem cell plasticity and drug tolerance. *Cell Stem Cell* **20**, 233–246 e7 (2017).
 - R. C. Allshire, H. D. Madhani, Ten principles of heterochromatin formation and function. *Nat. Rev. Mol. Cell Biol.* **19**, 229–244 (2018).
 - M. Sanchez-Martin, A. Ferrando, The NOTCH1-MYC highway toward T-cell acute lymphoblastic leukemia. *Blood* **129**, 1124–1133 (2017).
 - G. Troen, I. Wlodarska, A. Warsame, S. Hernández Llodrà, C. de Wolf-Peeters, J. Delabie, NOTCH2 mutations in marginal zone lymphoma. *Haematologica* **93**, 1107–1109 (2008).
 - A. S. Ho, K. Kannan, D. M. Roy, L. G. T. Morris, I. Ganly, N. Katabi, D. Ramaswami, L. A. Walsh, S. Eng, J. T. Huse, J. Zhang, I. Dolgalev, K. Huberman, A. Heguy, A. Viale, M. Drobnjak, M. A. Leversha, C. E. Rice, B. Singh, N. G. Iyer, C. R. Leemans, E. Bloemena, R. L. Ferris, R. R. Seethala, B. E. Gross, Y. Liang, R. Sinha, L. Peng, B. J. Raphael, S. Turcan,

- Y. Gong, N. Schultz, S. Kim, S. Chiosea, J. P. Shah, C. Sander, W. Lee, T. A. Chan, The mutational landscape of adenoid cystic carcinoma. *Nat. Genet.* **45**, 791–798 (2013).
48. S. Chen, J. Tao, Y. Bae, M.-M. Jiang, T. Bertin, Y. Chen, T. Yang, B. Lee, Notch gain of function inhibits chondrocyte differentiation via Rbpj-dependent suppression of Sox9. *J. Bone Miner. Res.* **28**, 649–659 (2013).
49. L. Chang, M. Nosedá, M. Higginson, M. Ly, A. Patenaude, M. Fuller, A. H. Kyle, A. I. Minchinton, M. C. Puri, D. J. Dumont, A. Karsan, Differentiation of vascular smooth muscle cells from local precursors during embryonic and adult arteriogenesis requires Notch signaling. *Proc. Natl. Acad. Sci. U.S.A.* **109**, 6993–6998 (2012).
50. Q. Xie, Q. Wu, L. Kim, T. E. Miller, B. B. Liaw, S. C. Mack, K. Yang, D. C. Factor, X. Fang, Z. Huang, W. Zhou, K. Alazem, X. Wang, B. E. Bernstein, S. Bao, J. N. Rich, RBPJ maintains brain tumor-initiating cells through CDK9-mediated transcriptional elongation. *J. Clin. Invest.* **126**, 2757–2772 (2016).
51. G. Zhang, S. Tanaka, S. Jiapaer, H. Sabit, S. Tamai, M. Kinoshita, M. Nakada, RBPJ contributes to the malignancy of glioblastoma and induction of proneural-mesenchymal transition via IL-6-STAT3 pathway. *Cancer Sci.* **111**, 4166–4176 (2020).
52. Q. Lv, R. Shen, J. Wang, RBPJ inhibition impairs the growth of lung cancer. *Tumour Biol.* **36**, 3751–3756 (2015).
53. T. Cardozo, M. Pagano, The SCF ubiquitin ligase: Insights into a molecular machine. *Nat. Rev. Mol. Cell Biol.* **5**, 739–751 (2004).
54. P. Barbosa, L. Zhaunova, S. DeBilio, V. Steccanella, V. Kelly, T. Ly, H. Ohkura, SCF-Fbxo42 promotes synaptonemal complex assembly by downregulating PP2A-B56. *J. Cell Biol.* **220**, (2021).
55. Z. Pillidge, S. J. Bray, SWI/SNF chromatin remodeling controls Notch-responsive enhancer accessibility. *EMBO Rep.* **20**, e46944 (2019).
56. M. J. Gomez-Lamarca, J. Falo-Sanjuan, R. Stojnic, S. A. Rehman, L. Muresan, M. L. Jones, Z. Pillidge, G. Cerda-Moya, Z. Yuan, S. Baloul, P. Valenti, K. Bystricky, F. Payre, K. O'H. Holleran, R. Kovall, S. J. Bray, Activation of the notch signaling pathway in vivo elicits changes in CSL nuclear dynamics. *Dev. Cell* **44**, 611–623.e7 (2018).
57. Q. Zhang, D. Karnak, M. Tan, T. S. Lawrence, M. A. Morgan, Y. Sun, FBXW7 facilitates nonhomologous end-joining via K63-linked polyubiquitylation of XRCC4. *Mol. Cell* **61**, 419–433 (2016).
58. H. van Attikum, S. M. Gasser, Crosstalk between histone modifications during the DNA damage response. *Trends Cell Biol.* **19**, 207–217 (2009).
59. N. E. Sanjana, O. Shalem, F. Zhang, Improved vectors and genome-wide libraries for CRISPR screening. *Nat. Methods* **11**, 783–784 (2014).
60. T. Tian, M. Bu, X. Chen, L. Ding, Y. Yang, J. Han, X.-H. Feng, P. Xu, T. Liu, S. Ying, Y. Lei, Q. Li, J. Huang, The ZATT-TOP2A-PICH axis drives extensive replication fork reversal to promote genome stability. *Mol. Cell* **81**, 198–211.e6 (2021).
61. H. S. Kaya-Okur, S. J. Wu, C. A. Codomo, E. S. Pledger, T. D. Bryson, J. G. Henikoff, K. Ahmad, S. Henikoff, CUT&Tag for efficient epigenomic profiling of small samples and single cells. *Nat. Commun.* **10**, 1930 (2019).
62. Y. Li, Z. Li, L. Dong, M. Tang, P. Zhang, C. Zhang, Z. Cao, Q. Zhu, Y. Chen, H. Wang, T. Wang, D. Lv, L. Wang, Y. Zhao, Y. Yang, H. Wang, H. Zhang, R. G. Roeder, W.-G. Zhu, Histone H1 acetylation at lysine 85 regulates chromatin condensation and genome stability upon DNA damage. *Nucleic Acids Res.* **46**, 7716–7730 (2018).
63. B. S. Nepon-Sixt, M. G. Alexandrow, DNase I chromatin accessibility analysis. *Bio Protoc.* **9**, e3444 (2019).
64. B. S. Nepon-Sixt, V. L. Bryant, M. G. Alexandrow, Myc-driven chromatin accessibility regulates Cdc45 assembly into CMG helicases. *Commun. Biol.* **2**, 110 (2019).
65. Q. Wang, W. Li, Y. Zhang, X. Yuan, K. Xu, J. Yu, Z. Chen, R. Beroukhi, H. Wang, M. Lupien, T. Wu, M. M. Regan, C. A. Meyer, J. S. Carroll, A. K. Manrai, O. A. Jänne, S. P. Balk, R. Mehra, B. Han, A. M. Chinnaiyan, M. A. Rubin, L. True, M. Fiorentino, C. Fiore, M. Loda, P. W. Kantoff, X. S. Liu, M. Brown, Androgen receptor regulates a distinct transcription program in androgen-independent prostate cancer. *Cell* **138**, 245–256 (2009).

Acknowledgments: We thank H. Shi, D. Li, and H. Yu for help, advice, and critical reading. We thank W. Plunkett, X. Liu, M. Antonio, and A. Beatriz for sharing human leukemia cell lines. We thank S. Tang for sharing healthy hematopoietic cells. We thank the Westlake University Supercomputer Center, Biomedical Research Core Facilities, Protein Characterization and Crystallography Facility, and Laboratory Animal Research Center for computational resources and related assistance. **Funding:** This work was supported by the Natural Science Foundation of China 91954103 (to X.L.) and an Institutional Startup Grant from the Westlake Education Foundation (to X.L.). **Author contributions:** X.L. and W.W. conceived the project. H.J., W.B., Y.S., H.L., and H.Z. performed the experiments and analyzed the data. H.J., W.B., Y.S., and X.L. wrote the manuscript. **Competing interests:** The authors declare that they have no competing interests. **Data and materials availability:** All data needed to evaluate the conclusions in the paper are present in the paper and/or the Supplementary Materials. Raw CUT&Tag-seq and ATAC-seq data have been deposited in the Gene Expression Omnibus (GEO) database under the accession code: GSE206985. The MS proteomics data have been deposited to the ProteomeXchange Consortium (<http://proteomecentral.proteomexchange.org>) via the PRIDE partner repository with the dataset identifier PXD034938 and 10.6019/PXD034938.

Submitted 11 April 2022

Accepted 4 August 2022

Published 21 September 2022

10.1126/sciadv.abq4831